Numerical modelling of tsunami inundation along the Kennedy Bay to Opito Bay coast, Coromandel Peninsula, New Zealand

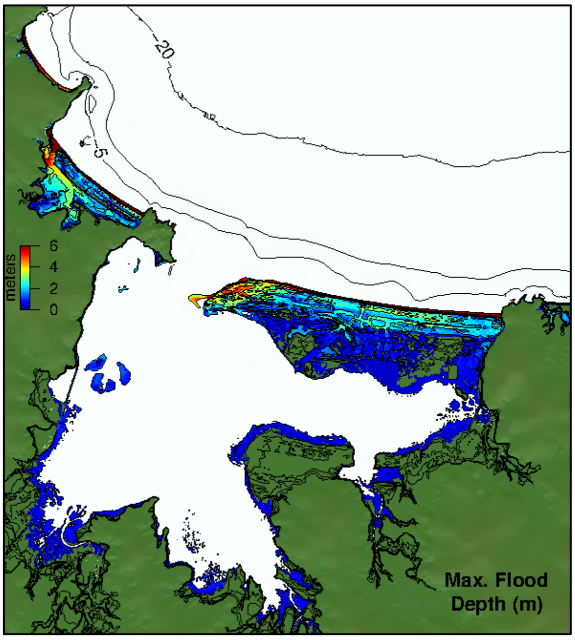

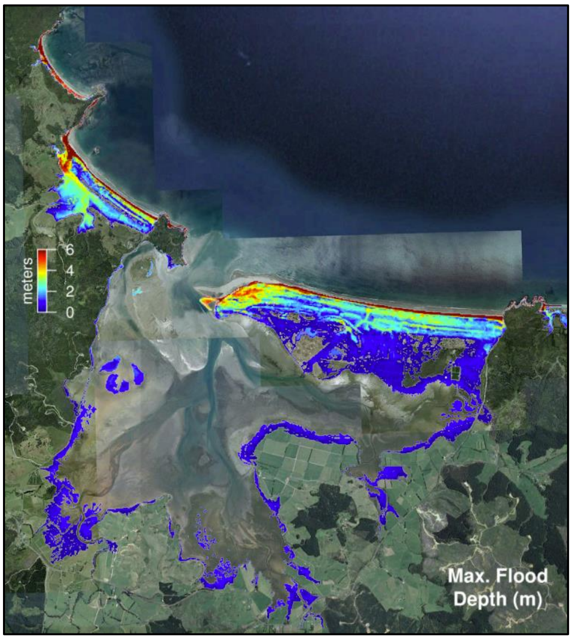

eCoast Limited
Marine Consulting and Research
P.O. Box 151
Raglan, New Zealand

jose@ecoast.co.nz

Numerical modelling of tsunami inundation along the Kennedy Bay to Opito Bay coast, Coromandel Peninsula, New Zealand

Report Status

Version	Date	Status	Approved By:
V 1	15-August-2015	DRAFT	JCB
V2	5-December-2015	FINAL	JCB/BM

It is the responsibility of the reader to verify the currency of the version number of this report.

Jose C. Borrero Ph.D.

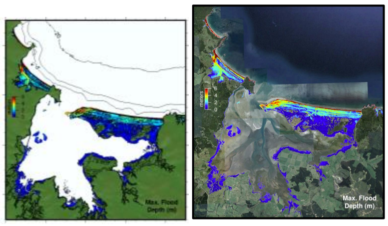

Cover Picture: Maximum overland flood depth at Matarangi and Whangapoua caused by tsunami source model 'Case 8' at High Tide (HT). Model Output (left) and over aerial imagery (right).

CONTENTS

TABLE OF FIGURES

TABLE OF TABLES

1 INTRODUCTION

This report describes the assessment of tsunami effects resulting from near source and distant source earthquake along the northern Coromandel Peninsula. This report focuses on the effects at Kennedy Bay, Whangapoua Beach, Whangapoua Harbour, Matarangi Beach, Rings Beach, Kuaotunu, Otama Beach and Opito Bay (Figure 1.1). Results presented here include the quantification of maximum and minimum tsunami wave heights, the extents of tsunami inundation and tsunami induced flood depths and the strength and duration of tsunami induced currents. The results from this study are intended to guide emergency management and evacuation planning activities. As such, this study focuses primarily on extreme tsunami scenarios in an effort to define likely maximum credible events for the purposes of planning evacuation routes and increasing public awareness. This report extends tsunami inundation and hazard studies previously completed by Borrero (2013, 2014). This work carries on from the work of Prasetya et al. (2008), who analysed near source and distant source tsunami inundation at Whitianga.

For the near source events, we consider a range of large magnitude (M>8.5) events located along the Tonga Kermadec trench, a subduction zone plate boundary between the Pacific and Australasian tectonic plates that extends from the east coast of the North Island to Tonga. For the distant source events, we consider only South American tsunamis for two reasons; firstly, sensitivity studies for Pacific Rim tsunamis conducted by Borrero et al. (2014) suggest that for a given earthquake size, tsunamis originating from South America have a larger impact in New Zealand than do tsunamis originating form most other parts of the Pacific Rim, and secondly, the South American Subduction Zone (SASZ) has a well-known history of producing very large earthquakes (>M8.5) and is likely to produce another such event in coming decades. While the sensitivity study of Borrero et al. (2014) show that tsunamis originating from Central America produce somewhat larger tsunami heights in New Zealand than a South American source of equivalent magnitude, the subduction zone offshore of Central America has never produced an earthquake with sufficient magnitude to generate a trans-pacific tsunami. For this reason, tsunamis from Central America are not considered here, nor are large magnitude events from other parts of the Pacific Rim. Given the historical record and the results from Borrero et al. (2014) we assume that the cases modelled here represent maximum credible event for distant source tsunamis.

We use the current state-of-the art tsunami modelling tools (ComMIT: Titov et al. 2011) and the most recent scientific literature on the relevant tsunami source mechanisms. Model results are compared quantitatively and qualitatively to available historical information.

Figure 1.1 Location map for the study sites. on the east coast of the Coromandel Peninsula.

1.1 Review of Recent Literature

As noted above, this study extends the work of Prasetya et al. (2008) and provides inundation estimates for additional areas along the Waikato east coast for both near source and distant source tsunamis.

Important results that came from the Prasetya et al. (2008) study include:

- Recognition of the importance of the source data for developing an accurate terrain model. They described the effect of terrain models derived from ground-striking and non-ground-striking LiDAR source data on tsunami inundation.

- Characterising the early onset hazard associated with Tonga-Kermadec trench sources.

- Assessing the relative severity of tsunami effects as it relates to the source mechanism and location.

Since the Work of Prasetya et al., (2008), an additional study by Prasetya and Wang (2011) investigated the recurrence of tectonic tsunami sources located along the Kermadec Trench and in the Bay of Plenty. Their analysis provides a suite of potentially tsunamigenic earthquake sources for the Kermadec Trench and is used as the basis for the modelling presented here.

1.2 Modelling Approach

The numerical modelling presented in this study was carried out using the Community Model Interface for Tsunamis (ComMIT) numerical modelling tool. The ComMIT model interface was developed by the United States government National Oceanic and Atmospheric Administration's (NOAA) Centre for Tsunami Research (NCTR) following the December 26, 2004 Indian Ocean tsunami as a way to efficiently distribute assessment capabilities amongst tsunami prone countries.

The backbone of the ComMIT system is a database of pre-computed deep water propagation results for tsunamis generated by unit displacements on fault plane segments (100 x 50 km) positioned along the world's subduction zones. Currently, there are 1,691 pre-computed unit source propagation model runs covering the world's oceans included in the propagation database. Using linear superposition, the deep ocean tsunami propagation results from more complex faulting scenarios can be created by scaling and/or combining the pre-computed propagation results from a number of unit sources (Titov et al., 2011). The resulting trans-oceanic tsunami propagation results are then used as boundary inputs for a series of nested near shore grids covering a coastline of interest. The nested model propagates the tsunami to shore computing wave height, velocity and overland inundation. The hydrodynamic calculations contained within ComMIT are based on the MOST (Method Of Splitting Tsunami) algorithm described in Titov and Synolakis (1995, 1997) and Titov and Gonzalez (1997). The ComMIT tool can also be used in conjunction with real time recordings of tsunami waveforms on one or more of the deep ocean tsunameter (DART) stations deployed throughout the oceans to fine tune details of an earthquake source mechanism in real time. An iterative algorithm that selects and scales the unit source segments is used until an acceptable fit to the observed DART data is met.

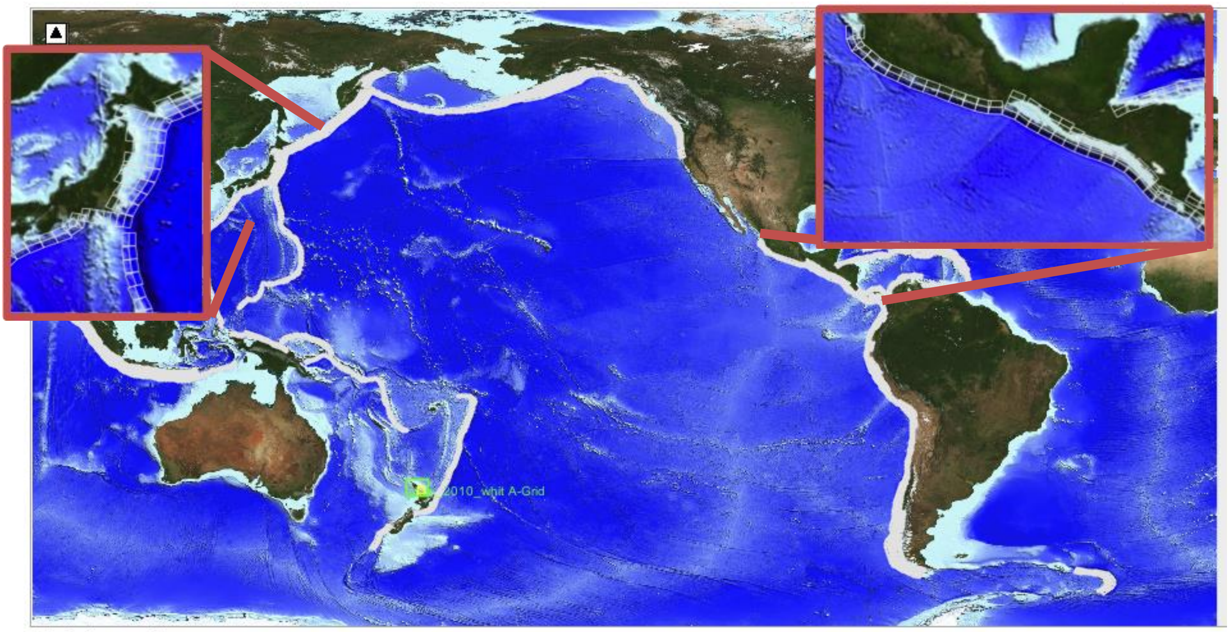

Figure 1.2 The ComMIT propagation model database for tsunamis in the world's oceans. Insets show the details of the source zone discretization in to rectangular sub-faults.

1.3 Numerical Modelling Grids

The Waikato Regional Council provided raw bathymetry and LiDAR topography data for construction of the numerical modelling grids. The data were provided with a reference datum of MSL and a WGS84 projection. The data were combined with additional data sets covering the regional offshore bathymetry and on land topography. This included the Shuttle Radar Topography Mission (SRTM) 90 m resolution topography, 200 m resolution bathymetry from NIWA, as well as nautical chart data from Land Information New Zealand (LINZ). The coverage areas of the various data sets are shown in Figure 1.3. The data were combined in to a master set of (x, y, z) triplets and then gridded in to different resolutions and coverage areas using a Kriging algorithm (Figure 1.4). Model grids were set up for both mean sea level (MSL) and mean high tide (HT).

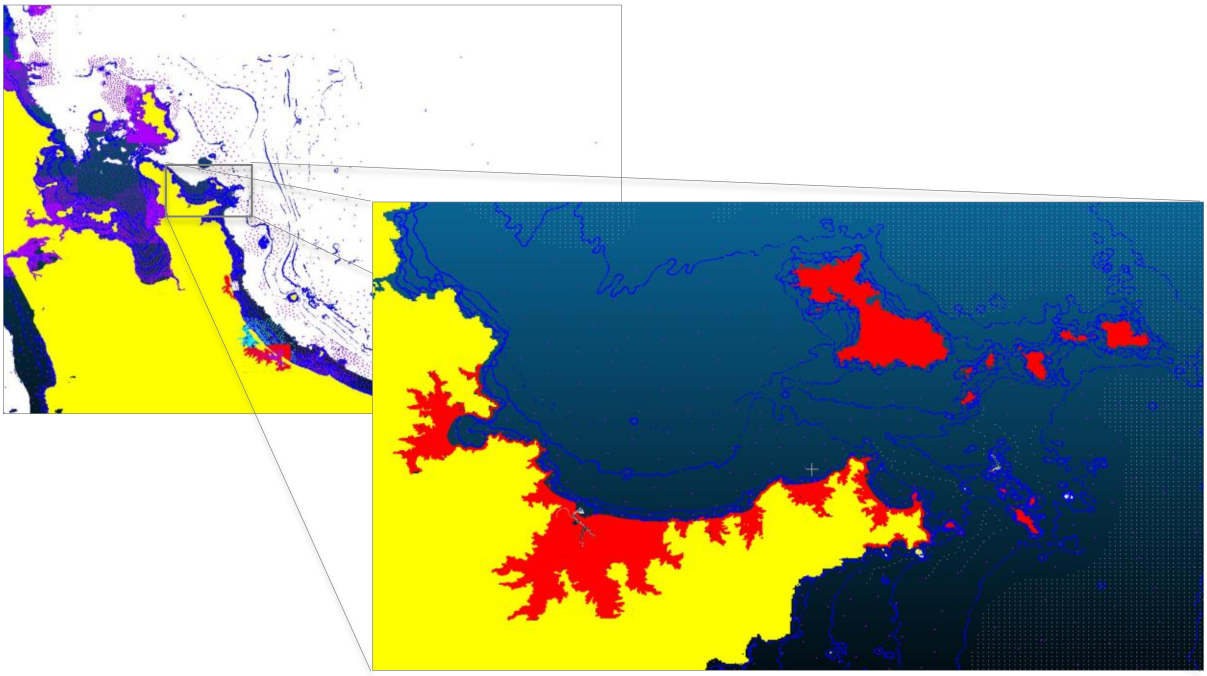

Figure 1.3 (left) coverage area of the different bathymetry data sets. Yellow: SRTM topography, White: NIWA bathymetry, Blue and Purple: LINZ digitised charts contours and sounding points. (right) Close-up of the Kennedy Bay/Whangapoua/Kuaotunu/Opito Bay region, yellow: SRTM topography, Red: LiDAR topography, Blue: LINZ digitized contours and soundings.

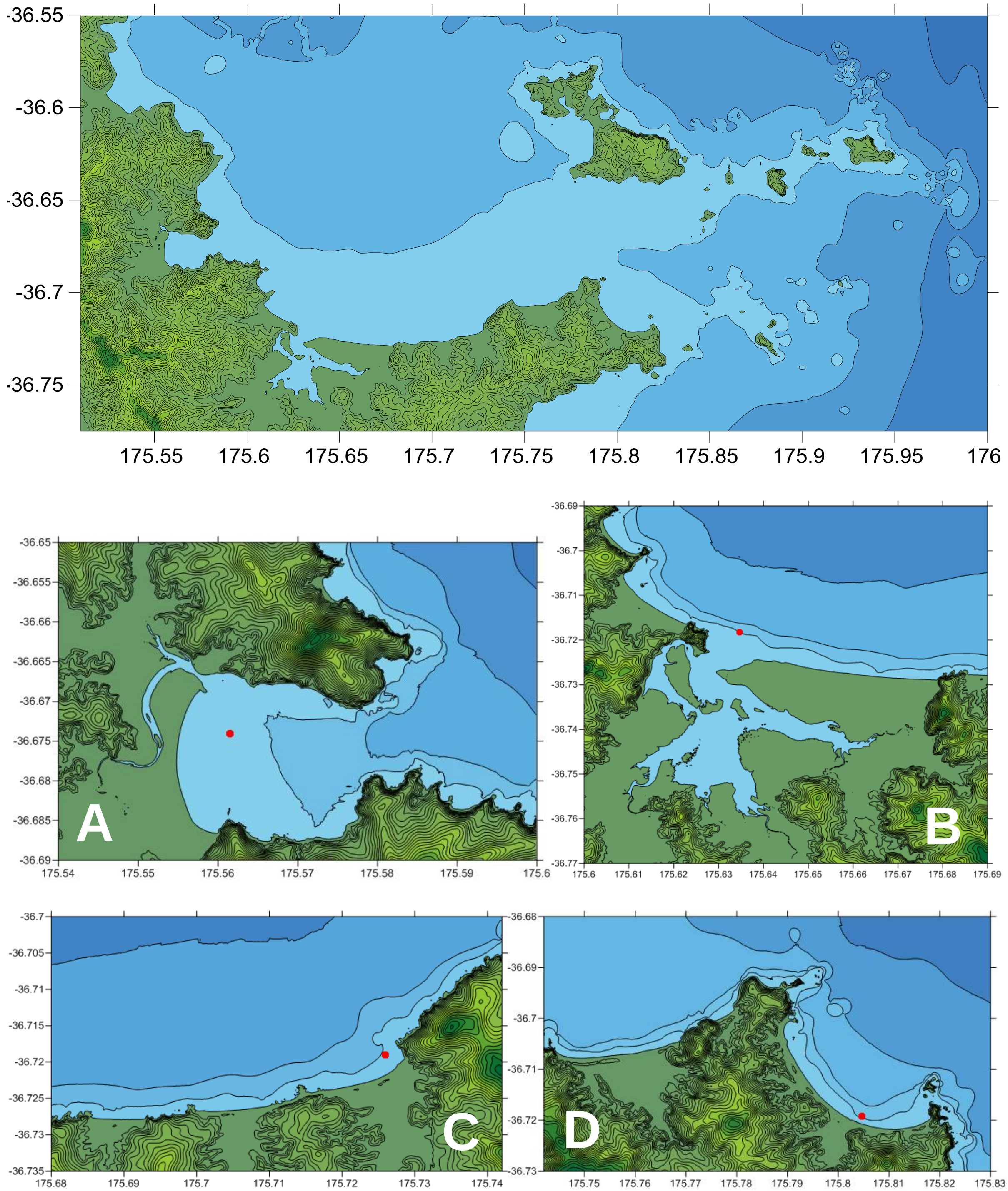

Figure 1.4 The final numerical modelling grids: B grid (top) at 150 m resolution and then clockwise from top left: A) Kennedy Bay B) Whangapoua and Matarangi Beaches and the Whangapoua Harbour C) Rings Beach, Kuaotunu and D) Otama Beach and Opito Bay at 10 m resolution. The red dot indicates location where water level time-series are extracted.

2 TSUNAMI SOURCE MODELS

For this study we focused on tsunamis generated by both near source and distant source tectonic events. For the near source scenarios, we use a range of hypothetical earthquakes on the Tonga-Kermadec trench, which lies to the east of New Zealand. For the distant source scenarios we explore the effects of historical events including the 1960 Valdivia, Chile earthquake, the 2010 Maule Chile earthquake and the 1868 Arica Chile earthquake. An additional set of scenarios looks at the relative hazard posed by an earthquakes similar to the 1960 event positioned along the coast of Northern Chile and Peru, in a locations that may be more favourable for wave energy transmission towards New Zealand (Power and Gale 2011).

2.1 Near Source Tonga-Kermadec Trench Scenarios

The Kermadec trench scenarios are based on the work presented in Prasetya and Wang (2011) and Power et al., (2011). In that study they presented a number of potential source mechanisms based on and extensive literature review of the tectonics of the Kermadec Trench. For this analysis, we used eight different source models; two M8.9 earthquake sources with ~10.5 m average slip, two M9 earthquake sources with 14.9 m of average slip, two M9.1 sources with 20.9 m of average slip and two cases replicating the variable slip distribution of the 2011 Tohoku earthquake (responsible for the great Pacific tsunami of March 11, 2011). The sources are shown in Figure 2.1 through Figure 2.3 and described in Table 2.1. Each of the sources is positioned at two locations; one situated some 200 km north of East Cape and the other extending from the northern tip of East Cape. The TK 8 scenario is regarded as a maximum credible event from the Tauranga-Kermadec Trench source area.

Table 2.1 Tsunami source models on the Tonga Kermadec Trench considered in this study.

Number	Source
TK 1	M 8.9, 10.5 m uniform slip, 600x100 km fault plane, 200 km north of East Cape
TK 2	M 8.9, 10.5 m uniform slip, 600x100 km fault plane, 0 km north of East Cape
TK 3	M 9.0, 14.8 m uniform slip, 600x100 km fault plane, 200 km north of East Cape
TK 4	M 9.0, 14.8 m uniform slip, 600x100 km fault plane, 0 km north of East Cape
TK 5	M 9.1, 20.9 m uniform slip, 600x100 km fault plane, 200 km north of East Cape
TK 6	M 9.1, 20.9 m uniform slip, 600x100 km fault plane, 0 km north of East Cape
TK 7	M 8.8, Variable slip model, equivalent to 2011 Tohoku tsunami source positioned 200 km north of East Cape
TK 8	M 8.8, Variable slip model, equivalent to 2011 Tohoku tsunami source positioned 0 km north of East Cape

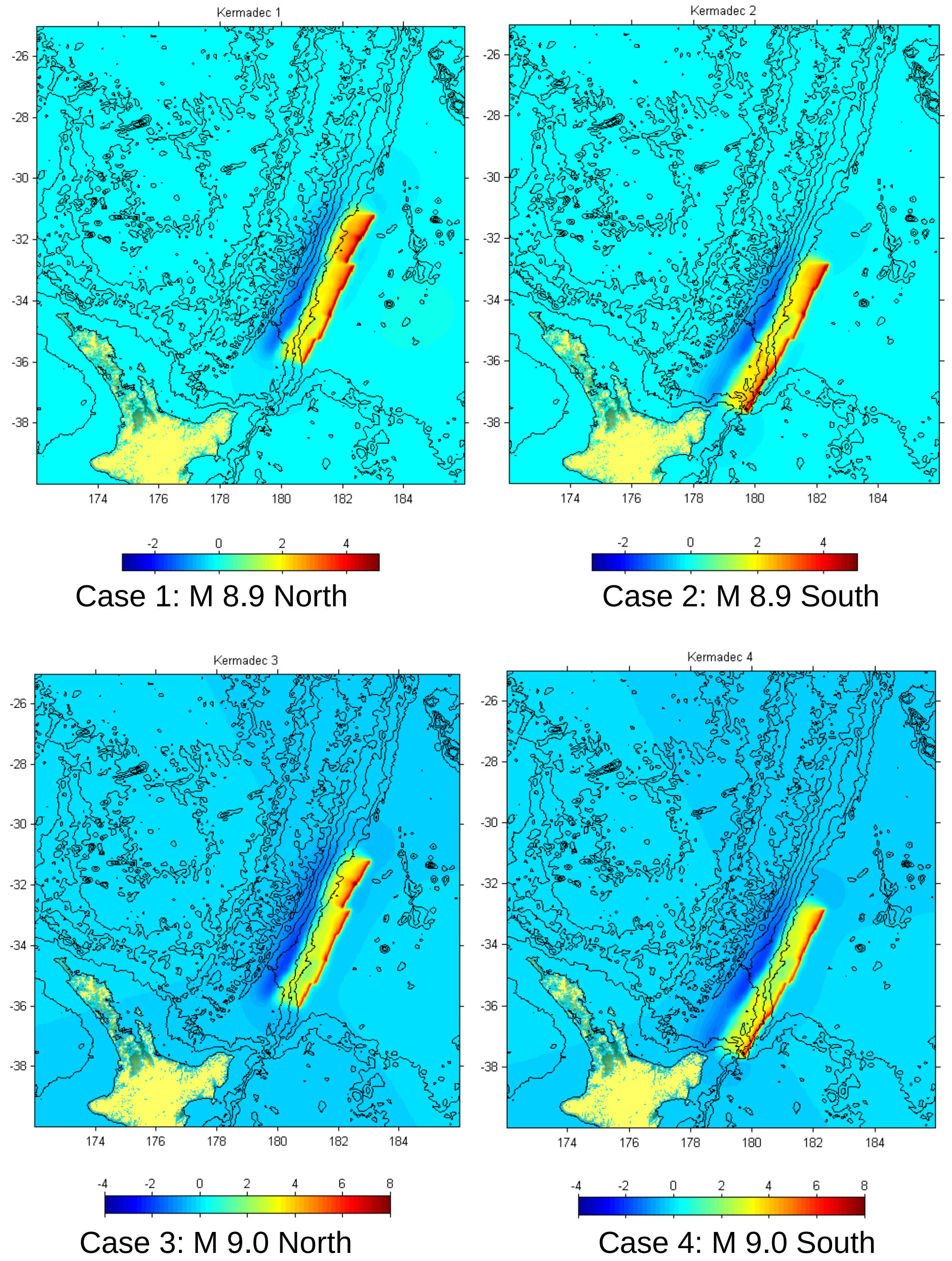

Figure 2.1 Case 1, 2: 600 x 100 km fault 10.47 m average slip, M = 8.9. Case 3, 4: 600 x 100 km fault, 14.8 m average slip, M = 9. Note the change in the colour scale for cases 3 and 4.

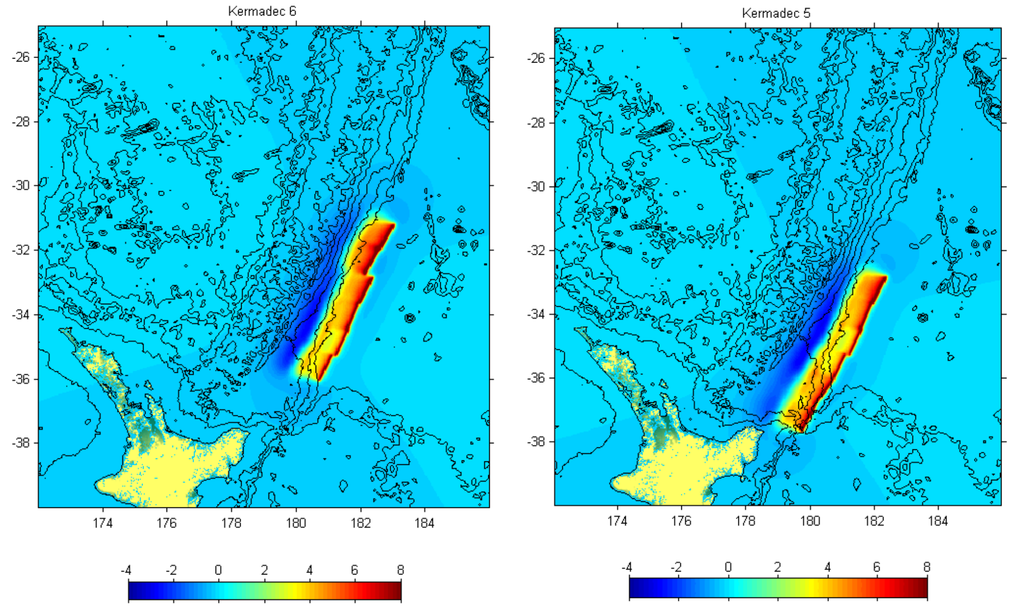

Figure 2.2 Cases 5 and 6: 600 x 100 km fault, 20.9 m average slip, M = 9.1

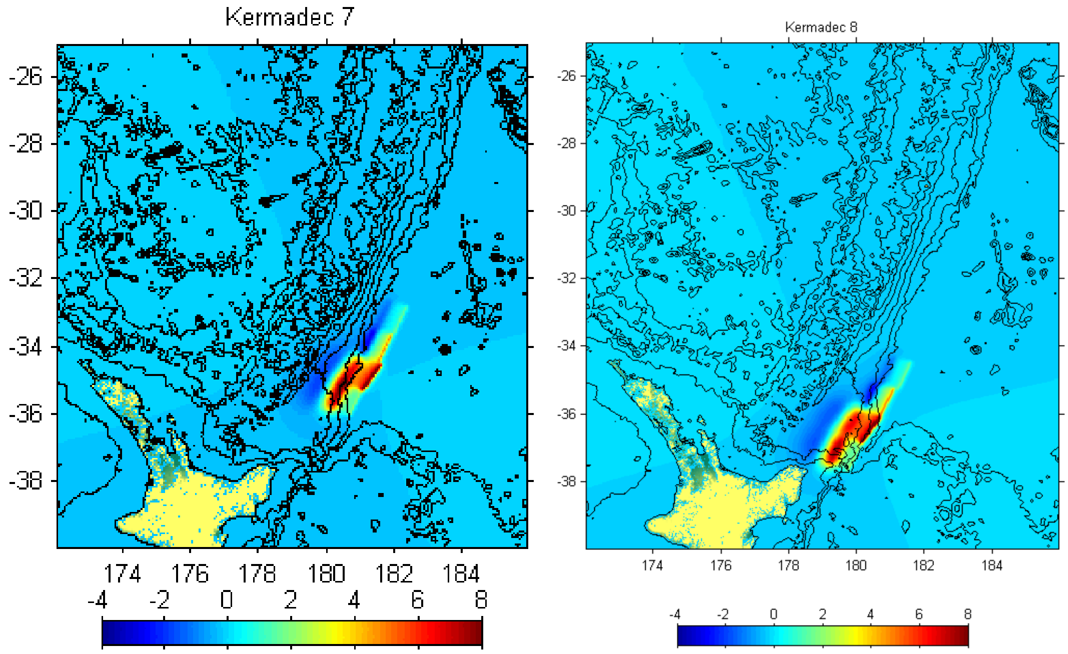

Figure 2.3 Case 7 (left) the Japan 2011 tsunami source positioned 200 km north of the East Cape (M = 8.8). Case 8 (right) the Japan 2011 tsunami source positioned at the southern end of the Tonga-Kermadec Trench (M=8.8).

2.2 Distant Source Tsunami Models

In total, seven distant source events considered. Three are based on historical events (1868 Arica, 1960 Valdivia and 2010 Maule). The four additional sources are derived from the source model for the 1960 Valdivia earthquake but are positioned at different locations and with different slip distributions. The sources are listed in Table 2.2 and described in the sections below. The FF 7 scenario is regarded as a maximum credible event for distant source tsunami.

Table 2.2 Description of the distant source tsunami scenarios.

Number	Source
FF 1	The 1960 Valdivia, Chile earthquake. Source model based on Fujii and Satake (2012)
FF 2	The 2010 Maule, Chile earthquake, source derived from NOAA real-time tsunameter inversion.
FF 3	1868 Arica – A very large magnitude event extending from Arica, Chile 600 km northward into southern Peru. Source uses uniform slip of xx m over the fault plane.
FF 4	Chile North 1 – A variant of the Fuji and Satake (2012) source for the 1960 tsunami modified to concentrate largest amounts of slip towards the north of the fault rupture and positioned such that the deformation region runs from northern Chile towards the south,
FF 5	Chile North 2– A variant of the Fuji and Satake (2012) source for the 1960 tsunami modified to concentrate largest amounts of slip towards the north of the fault rupture and positioned such that the deformation region straddles the Peru/Chile border with the largest deformation occurring offshore of southern Peru
FF 6	Chile North 3– A variant of the Fuji and Satake (2012) source for the 1960 tsunami modified to concentrate largest amounts of slip towards the south of the fault rupture and positioned such that the deformation region straddles the Peru/Chile border with the largest deformation occurring offshore of northern Chile.
FF 7	Peru – A variant of the Fuji and Satake (2012) source for the 1960 tsunami modified to concentrate largest amounts of slip towards the south of the fault rupture and positioned along the coast of Central Peru.

2.3 Historical Scenarios: 1960 Valdivia, 2010 Maule and 1868 Arica Earthquakes and Tsunamis

Two modern historical tsunami events are modelled in this study; the first is the 1960 Valdivia, Chile earthquake and the second is the 2010 Maule, Chile earthquake. Of the two, the 1960 event, which occurred in southern Chile, was much larger in terms of the earthquake magnitude and the tsunami height both in the near and far-field.

Borrero (2013) conducted a detailed analysis of the effects of the 1960 tsunami at Whitianga. In that study he compared the numerical model results from 6 different versions of the tsunami source for that event to eyewitness accounts and observations of inundation at Whitianga. The results of that study suggested that the earthquake slip distribution proposed by Fujii and Satake (2012) provided the best fit to the overall observed effects. However, it was necessary to increase the overall slip amounts by 20% to most accurately reproduce the observed inundation. The fault segments, initial seafloor deformation and slip amounts used for that source are shown in Figure 2.4 and Table 2.3.

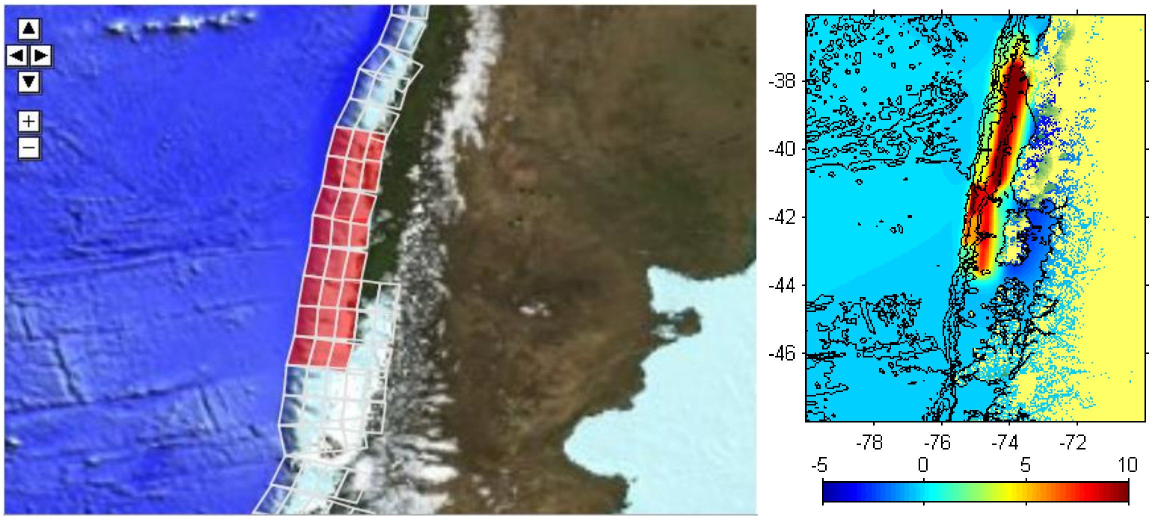

Figure 2.4 (left) Unit source segments used to define the 1960 Chilean Earthquake suite of events. (right) initial sea floor deformation at the source region.

Table 2.3 Faults segment slip amounts for the 1960 Chilean tsunami.

Fault Segment Slip Amounts		
5.0	12.9	1.2
6.6	36.1	21.0
2.8	31.1	11.3
4.9	29.6	11.5
7.8	32.9	6.6
25.7	17.8	6.2
15.3	21.7	5.5
3.7	20.5	2.7

On February 27, 2010 an earthquake with a moment magnitude (M_W) of 8.8 (United States Geological Survey) occurred in the coastal area of southern Chile. The earthquake caused a destructive tsunami in Chile and a moderate tsunami that was observed throughout the Pacific Ocean. The tsunami was clearly evident along the Coromandel Peninsula and resulted in the closure of the Whitianga Marina for 2 days. The source mechanism used for this simulation (Figure 2.5) was determined through the inversion of DART tsunameter data (NOAA/PMEL, pers. comm.). This source model was used to model tsunami heights in Whitianga and produced results consistent with measured water levels (Figure 2.6).

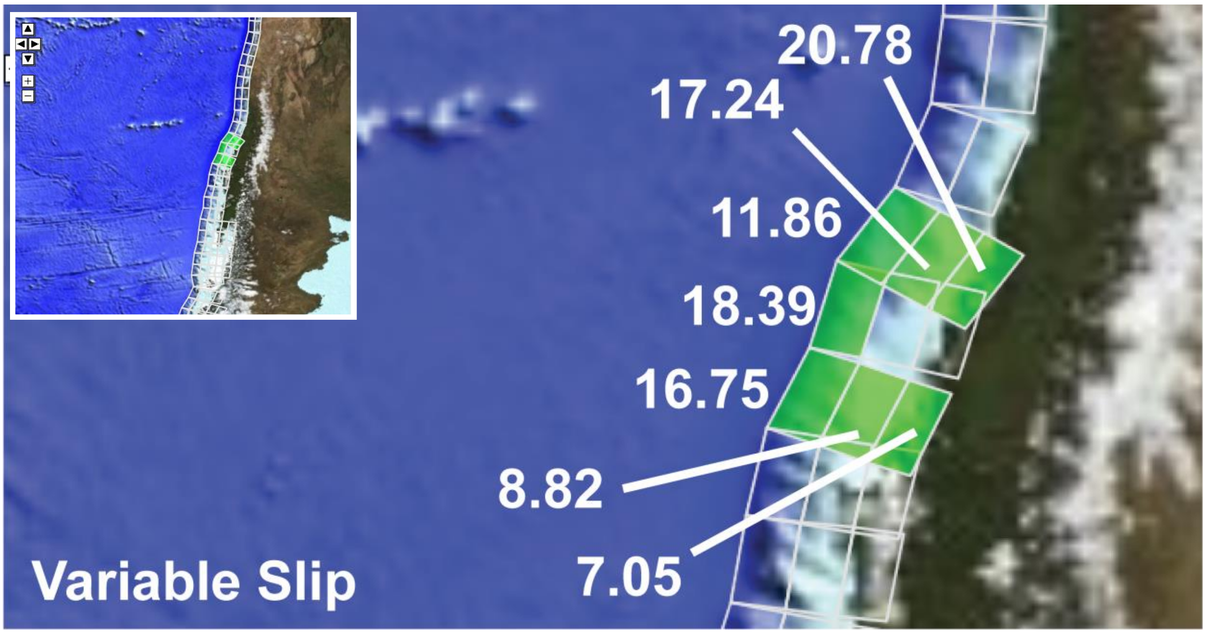

Figure 2.5 Source segments and slip amounts used to model the 2010 Chile tsunami.

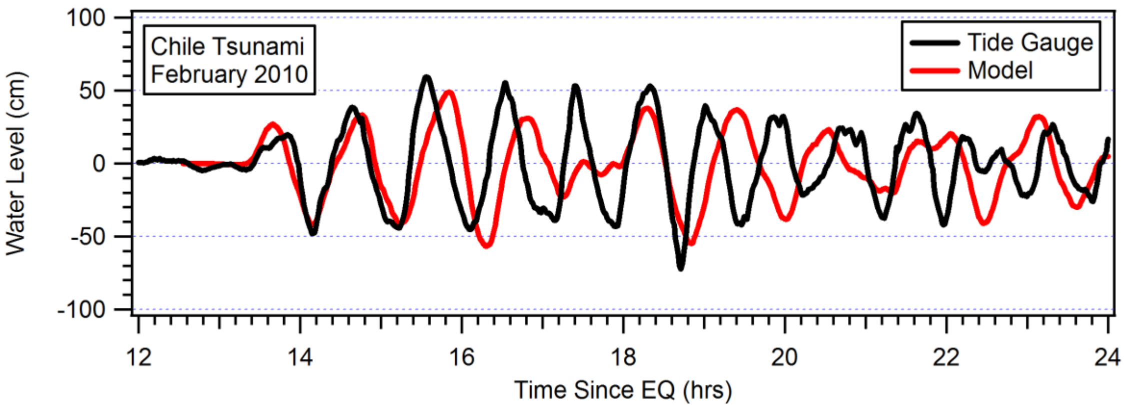

Figure 2.6 Comparison between measured and modelled water levels at the Whitianga tide gauge for the February 2010 Chile earthquake and tsunami.

The third historical tsunami event we consider is that of 13 August 1868. While there were no instrumental recordings of this tsunami, there are detailed accounts of the wave effects in New Zealand (de Lange and Healey, 1986). It is interesting to note that the effects on the North Island seem to be less severe than those on the South Island, with reported tsunami heights of 1-2 m at Mount Maunganui, Great Barrier Island and in the Tamaki Estuary. Even at Port Charles, the tsunami was only described as 'a high tide'. This is in contrast to the effects a Lyttelton Harbour near Christchurch, where the observations of Gibson (1868) suggested a peak to trough tsunami height of ~7.6 m (25 feet) for the first tsunami wave. To model this event, we based our tsunami source on the rupture length estimate of 600 km presented in Dorbath et al., (1990). Using fault segments extending from Arica northward (Figure 2.7) the model is initialized with a uniform slip amount of 39.6 m. Borrero and Goring (2015) showed that this amount of slip was necessary to replicate the observed 7 m water level change described by Gibson (1868).

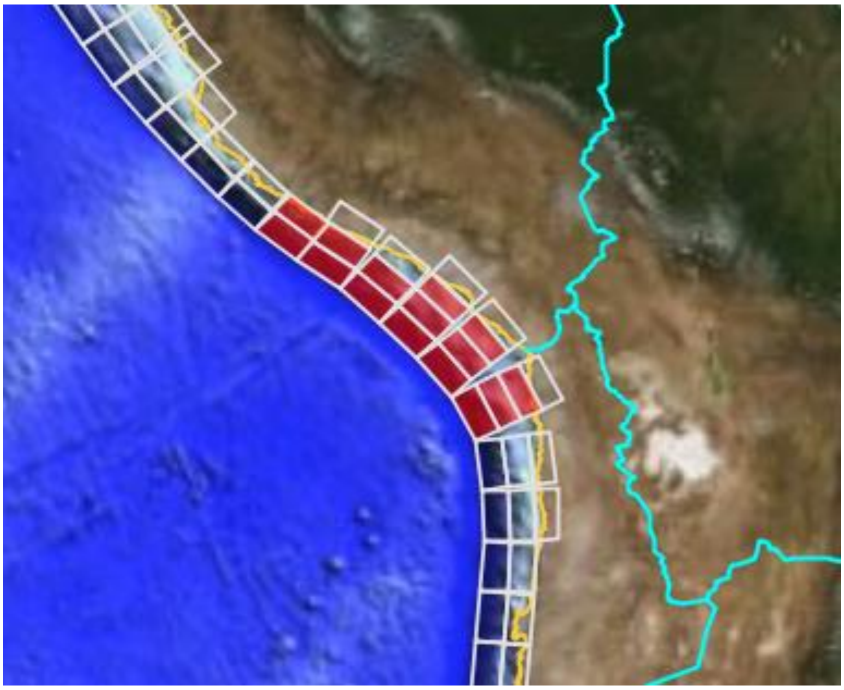

Figure 2.7 Source segments used to model the 1868 Arica tsunami. A uniform slip amount of 39.6 m was applied to each segment.

2.4 Additional South American Tsunami Sources: Peru and Northern Chile

Power et al. (2007) and Power and Gale (2012) showed that along the South American Subduction Zone, tsunamis generated along the Peru-Chile Border region have a greater impact along the New Zealand coast relative to sources located further to the north or south. Indeed, the 1960 event would have been more damaging in New Zealand had it occurred a few thousand km to the north. Furthermore the1868 event generated run-up of 1 – 4 m in New Zealand (up to 10 m in the Chatham Islands) and resulted in New Zealand's only tsunami related fatality since European settlement. The event caused damage to boats and infrastructure along the east coast of the North and South Islands. This event was followed 11 years later by another earthquake of similar magnitude (~M8.8) located further south along the northern coast of Chile. This event however was not as damaging or well observed in New Zealand as the 1868 event. For this reason we felt it was prudent to explore the effects of such an event. The source models we used were based on source model for the 1960 Chilean earthquake described by Fujii and Satake (2012). However, Borrero (2013), showed that the Fujii and Satake slip amounts should be increased by 20% to match the inundation observed in Whitianga. He also showed that by aggregating the high slip regions together, the resultant tsunami in New Zealand was larger. Therefore, to better represent a maximum credible event, this study uses the higher slip amounts with the high slip areas clustered together. These source models were then positioned at different locations along the South American Subduction Zone to assess the impacts at the study sites.

We first start with scenarios positioned near the Peru-Chile border. For Distant Source 4 (FF4), we first position the Fujii and Satake (2012) source model towards the north of Chile. This source has the high slip regions clustered to the north of the earthquake rupture area. For source FF5, this same deformation pattern is shifted

600 km to the north. For source FF6, we use the same segments as FF5 and reverse the deformation pattern to concentrate the slip to the south. The initial sea floor deformations used to initialize the hydrodynamic model are shown in Figure 2.9. The final distant source (FF7) is identical to FF6 with the entire deformation pattern shifted approximately 800 km north along the coast and situated off the coast of central Peru. This source also concentrates the high slip region to the south of the rupture area.

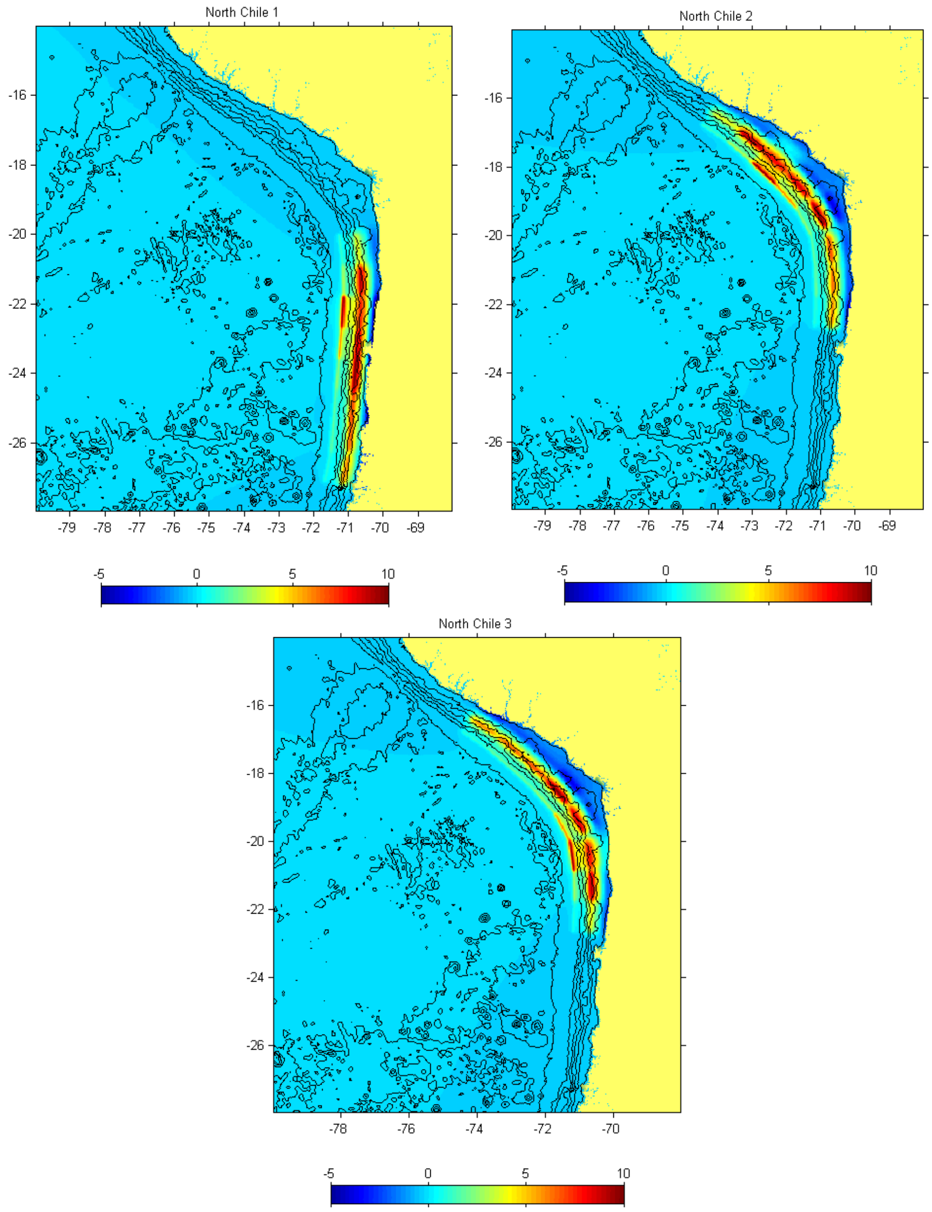

Figure 2.8 Three additional South American sources. Variants of the Fujii and Satake (2012) source for the 1960 Chile earthquake are positioned along the coast of Northern Chile and Southern Peru.

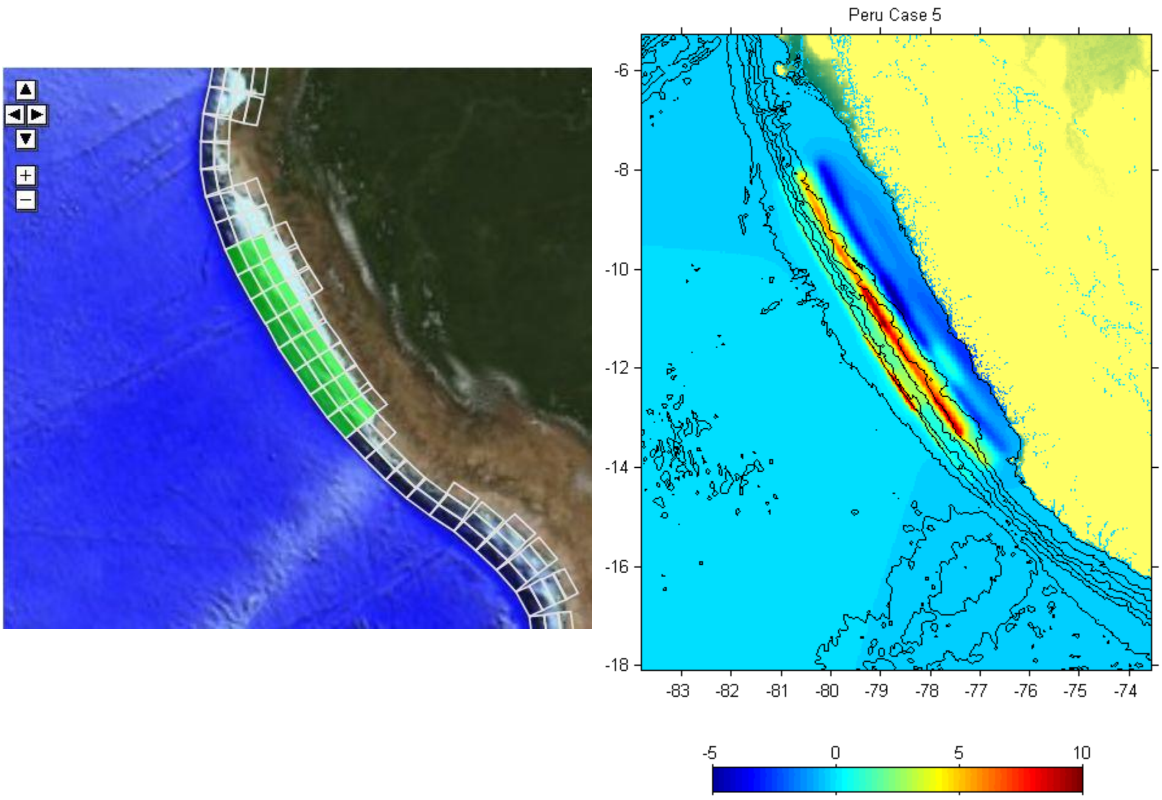

Figure 2.9 Fault segments used to construct the Peru tsunami source (left) and the initial deformation field used to initialise the tsunami model (right).

3 MODEL RESULTS: TONGA-KERMADEC TRENCH SOURCES

3.1 Arrival Times

An important consideration for the near source tsunami hazard is a clear understanding of the tsunami arrival time. ‘Tsunami arrival’ however can be defined in a number of ways whether it is the time of the first water motions (rise or drop) or the time of the maximum wave height. For the TK Trench source, we depict the tsunami arrival times in Figure 3.1 for the sources located further north and Figure 3.2 for the southern sources. In these plots we see that the first withdrawal of the water surface begins approximately 1 hour after the earthquake for the northern sources and slightly earlier for the southern sources. In some cases the initial withdrawal is followed by the largest positive surge, however in other cases significant surges continue for several hours after tsunami arrival. This is in contrast to the results from sites on the eastern shore of the Coromandel (i.e. Whangamata, Whiritoa, Tairua and Pauanui) where the modelled time series generally features a first surge that was much larger than subsequent surges. Furthermore, the modelled time series for the sites in this study are generally much larger than for the sites previously modelled. This may be due to the fact that these sites are located in a more exposed location towards the northern end of the Coromandel Peninsula.

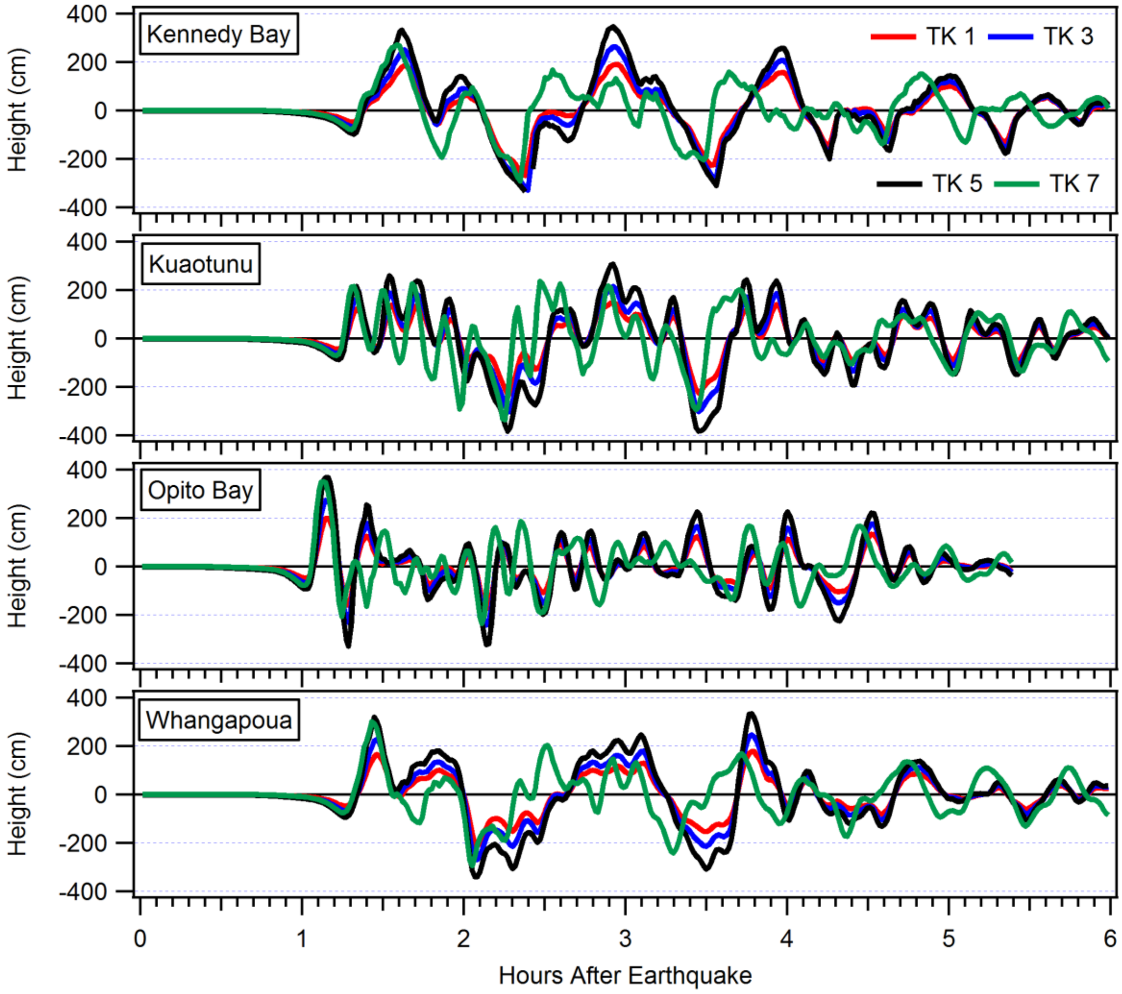

Figure 3.1 Water level time series plots for sources 1, 3, 5 and 7 at the four sites. Time series locations are indicated with the red dot in Figure 1.4.

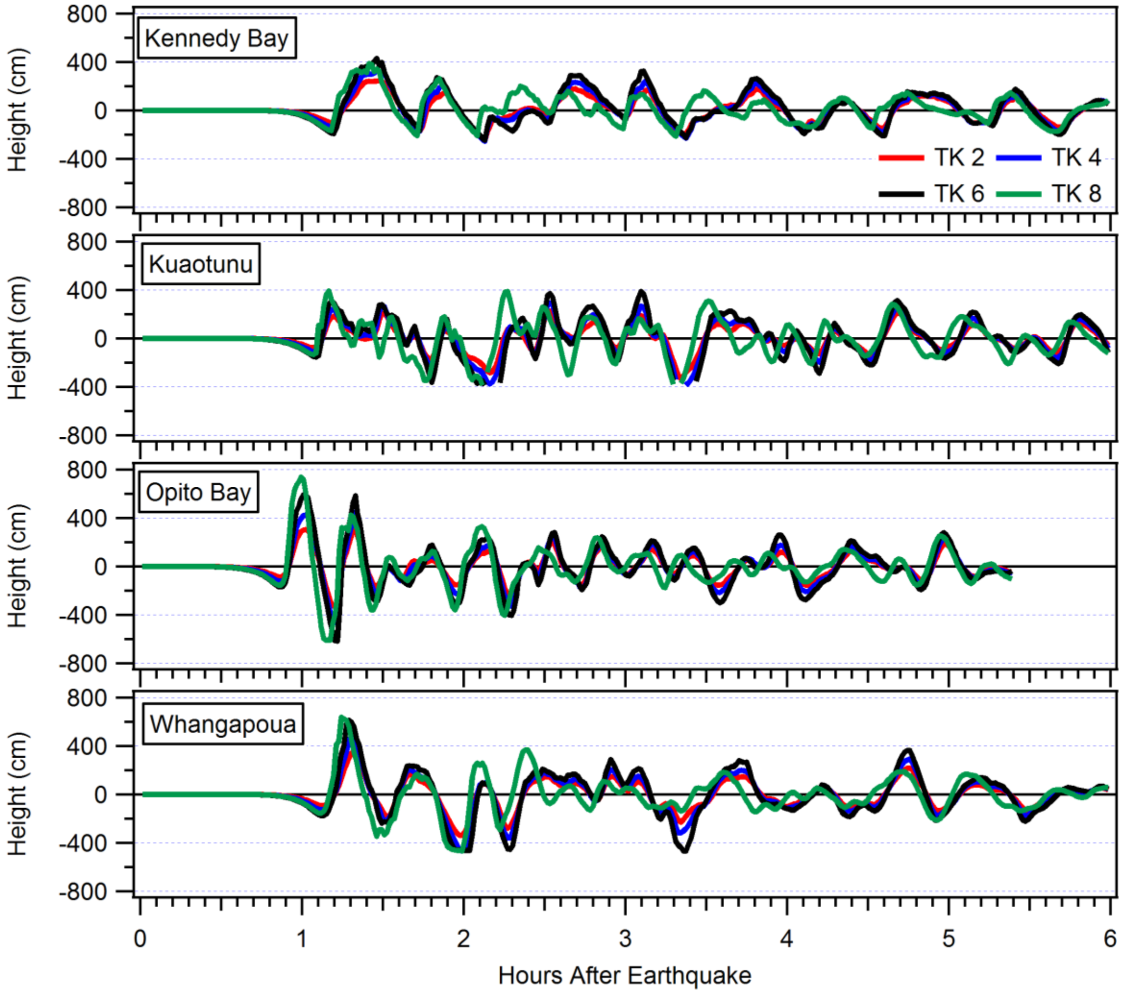

Figure 3.2 Water level time series plots for sources 2, 4, 6, and 8 at the four sites. Time series locations are indicated with the red dot in Figure 1.4.

3.2 Tsunami Height

For each of the tsunami source models, we simulated the tsunami inundation and current speeds for cases at mean sea level (MSL). Select cases were simulated at high tide (HT). The most obvious difference in the model results at the study sites however was a result of the location of the seafloor deformation. For sources located to the south, the tsunami induced wave heights were larger than for the sources positioned to the north. This effect was illustrated in Borrero (2013) by showing the wave height produced offshore of the Coromandel Peninsula by identical tsunami generated on 11 different fault segments running from the East Cape northward along the TK Trench. The results (reproduced in Figure 3.3) show that the wave height offshore of the Coromandel is very sensitive to the source location with wave heights dropping off rapidly as the earthquake deformation is moved further north. The strongest effects result from ruptures occurring just north of East Cape.

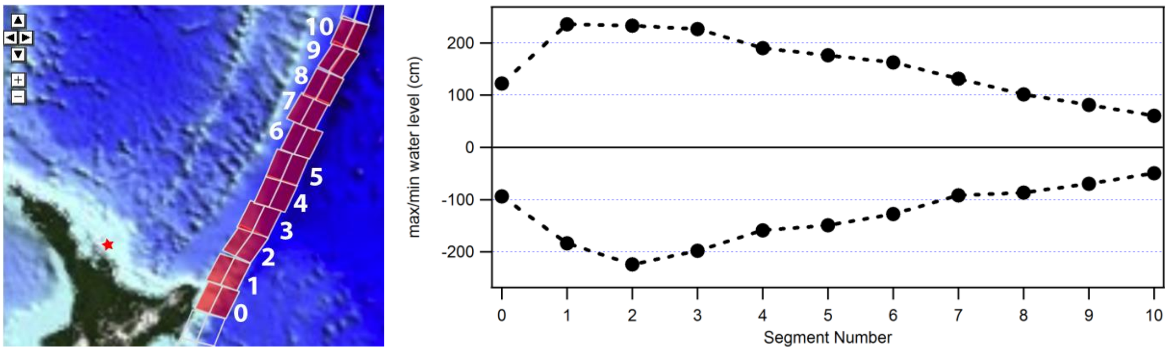

Figure 3.3 Tsunami wave heights produced offshore of the Coromandel Peninsula (red star) by identical tsunami sources positioned on each of the fault segments indicated in the panel on the left. Note that the strongest effects are the result of ruptures in the first 300 km north of the East Cape (segments 1, 2 and 3).

This effect can be seen in the coarse grid propagation plots shown in Figure 3.4 for source TK 1 and TK 2 with the corresponding near shore maximum water levels shown in Figure 3.5. Although neither of these cases results in significant inundation at Kennedy Bay, Whangapoua, Kuaotunu or Opito Bay, it is evident that the wave heights offshore of the Coromandel Peninsula from the southern TK2 scenario are larger. Of the sources modelled in this study, sources TK 6 and TK 8 produce the most significant inundation at the study sites. The inundation extents for these cases are shown in Figure 3.6 and Figure 3.7.

To illustrate the effect of high tide levels on the inundation extents, we ran the TK 8 scenario at high tide. As expected this resulted in greater inundation extents and deeper flood depths. The tsunami flood depths for cases TK8 and TK8 High Tide at Kennedy Bay, Whangapoua, Kuaotunu and Opito Bay are plotted over aerial imagery and compared in in Figure 3.13 through Figure 3.16 we present the overland inundation flood depth (in meters) for the TK 8 high tide scenarios.

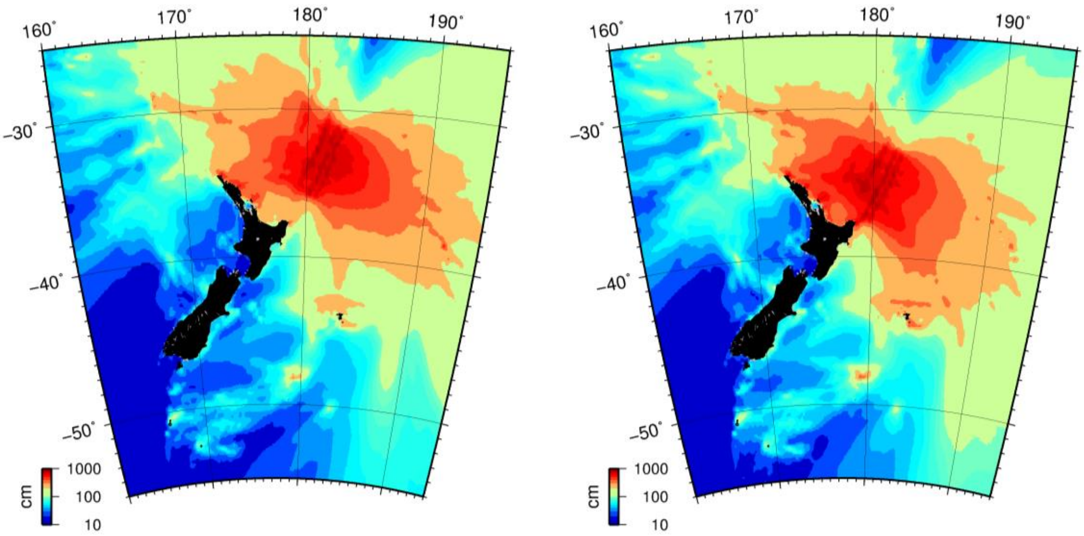

Figure 3.4 Maximum computed tsunami heights over the regional grid for source TK 1 (left) and TK 2 (right). Tsunami heights along the Coromandel Peninsula and in the Bay of Plenty are noticeably higher from source TK 2 due to its more southerly position along the subduction zone.

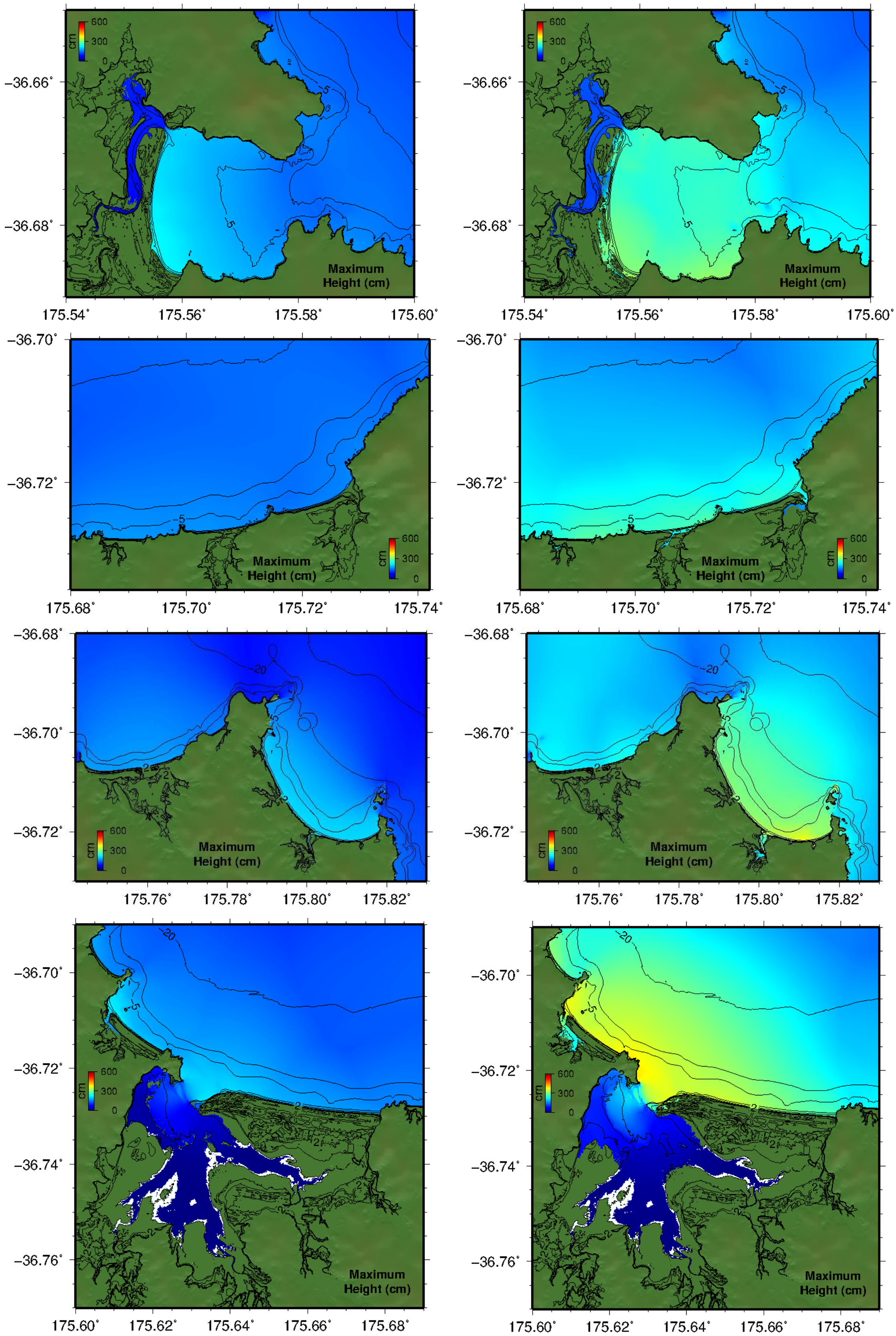

Figure 3.5 Maximum computed water levels for scenarios TK 1 (left) and TK 2 (right) at Kennedy Bay, Whangapoua, Kuaotunu and Opito Bay (top to bottom respectively); each case run at MSL.

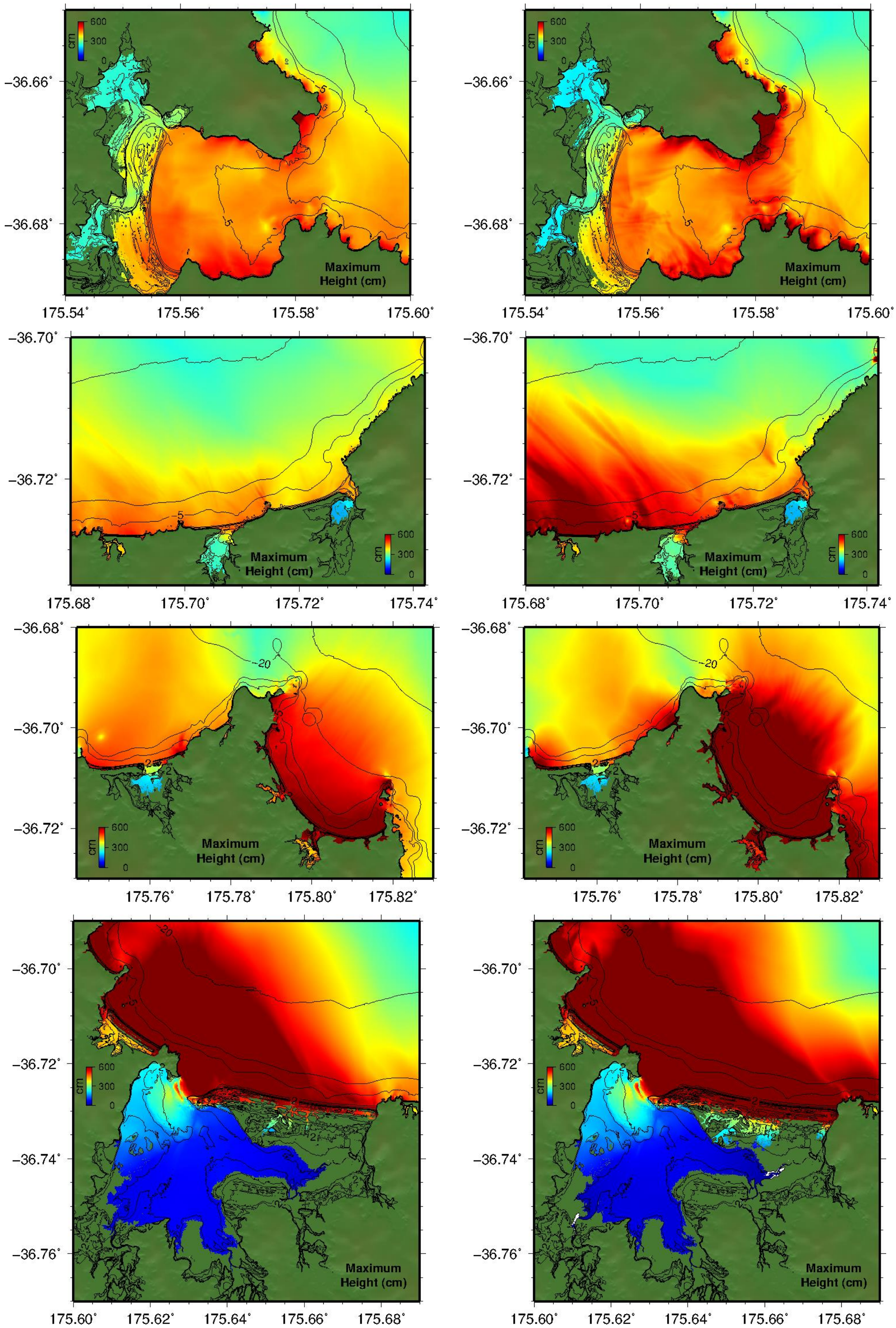

Figure 3.6 Maximum computed tsunami heights above model reference water level for scenarios TK 6 (left) and TK 8 (right) at Kennedy Bay, Whangapoua, Kuaotunu and Opito Bay (top to bottom respectively); each case run at MSL.

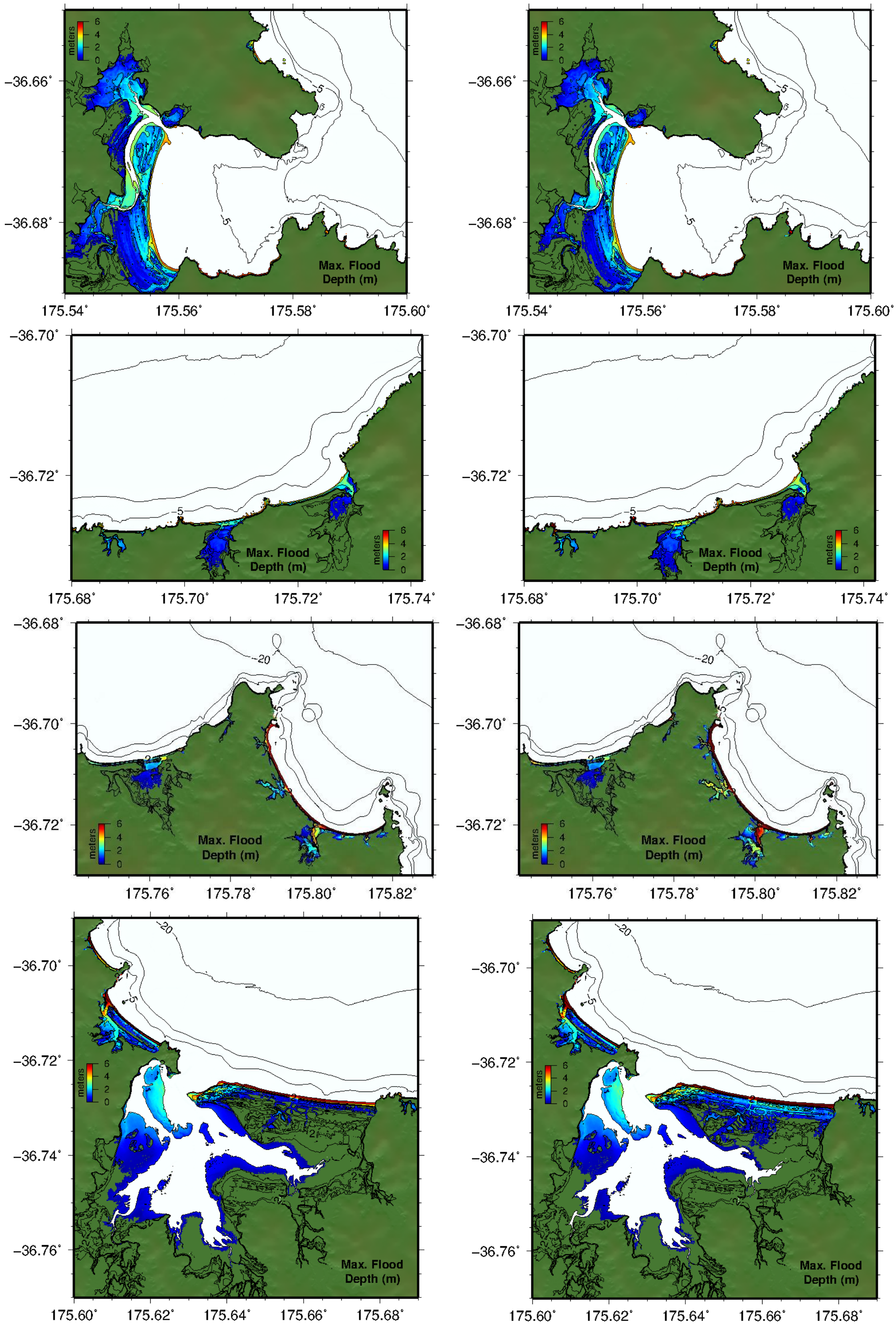

Figure 3.7 Maximum computed tsunami flood depths above ground level for scenarios TK 6 (left) and TK 8 (right) at Kennedy Bay, Whangapoua, Kuaotunu and Opito Bay (top to bottom respectively); each case run at MSL.

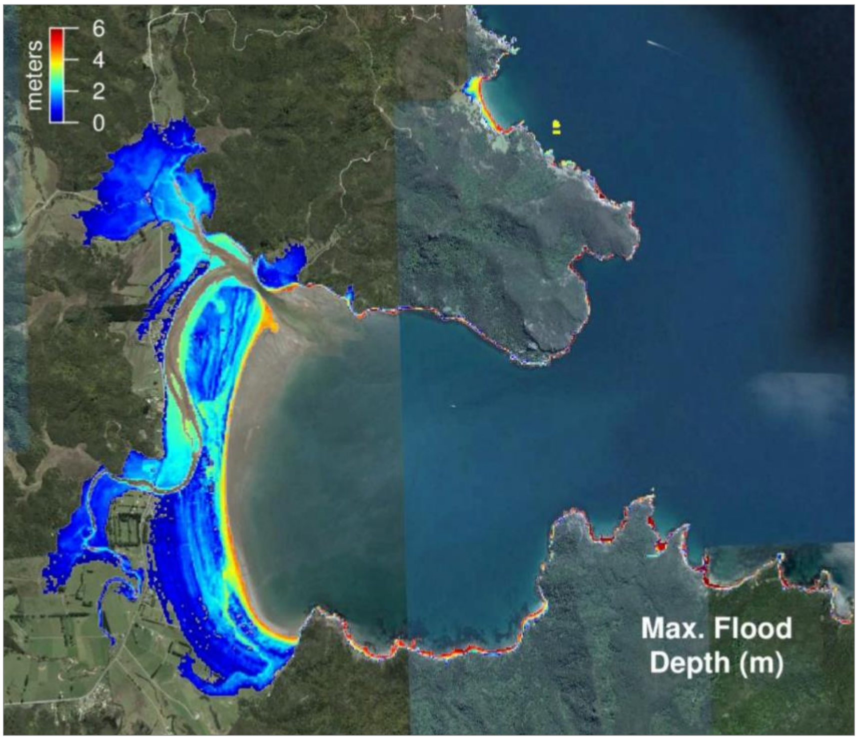

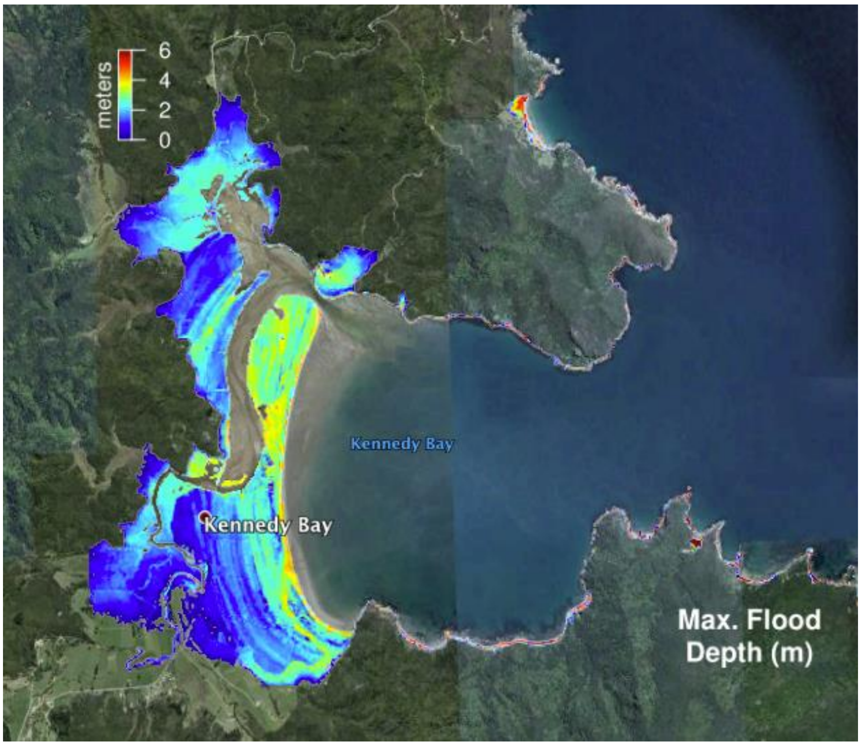

Figure 3.8 Maximum computed tsunami flood depths above ground level at Kennedy Bay for scenario TK 8 MSL (top) and TK 8 HT (bottom).

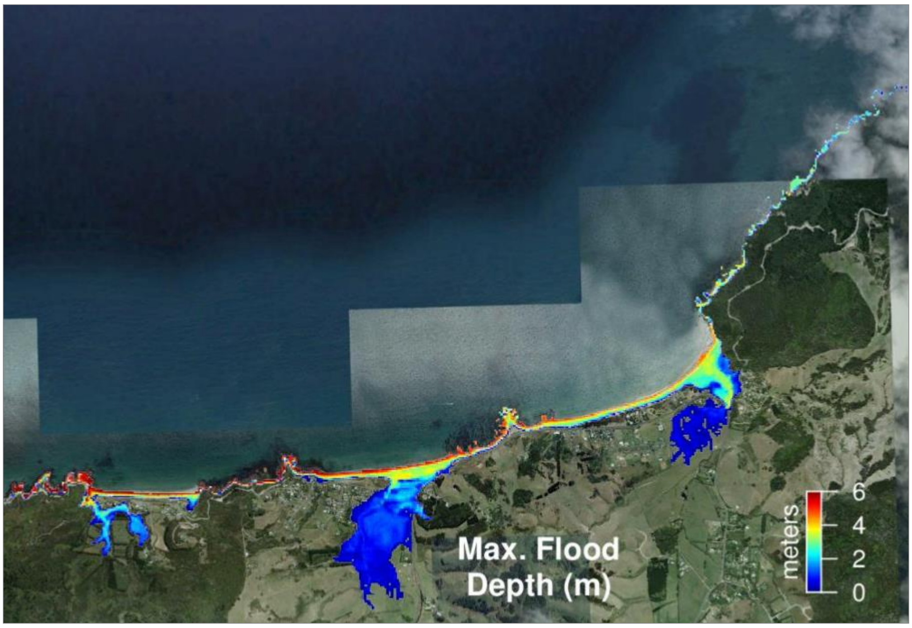

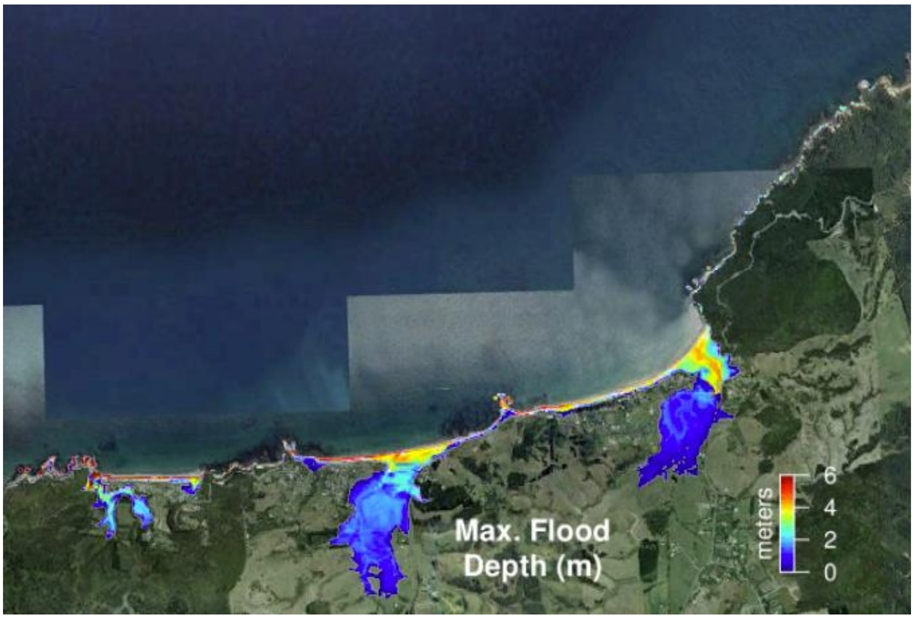

Figure 3.9 Maximum computed tsunami flood depths above ground level at Kuaotunu for scenario TK 8 MSL (top) and TK 8 HT (bottom).

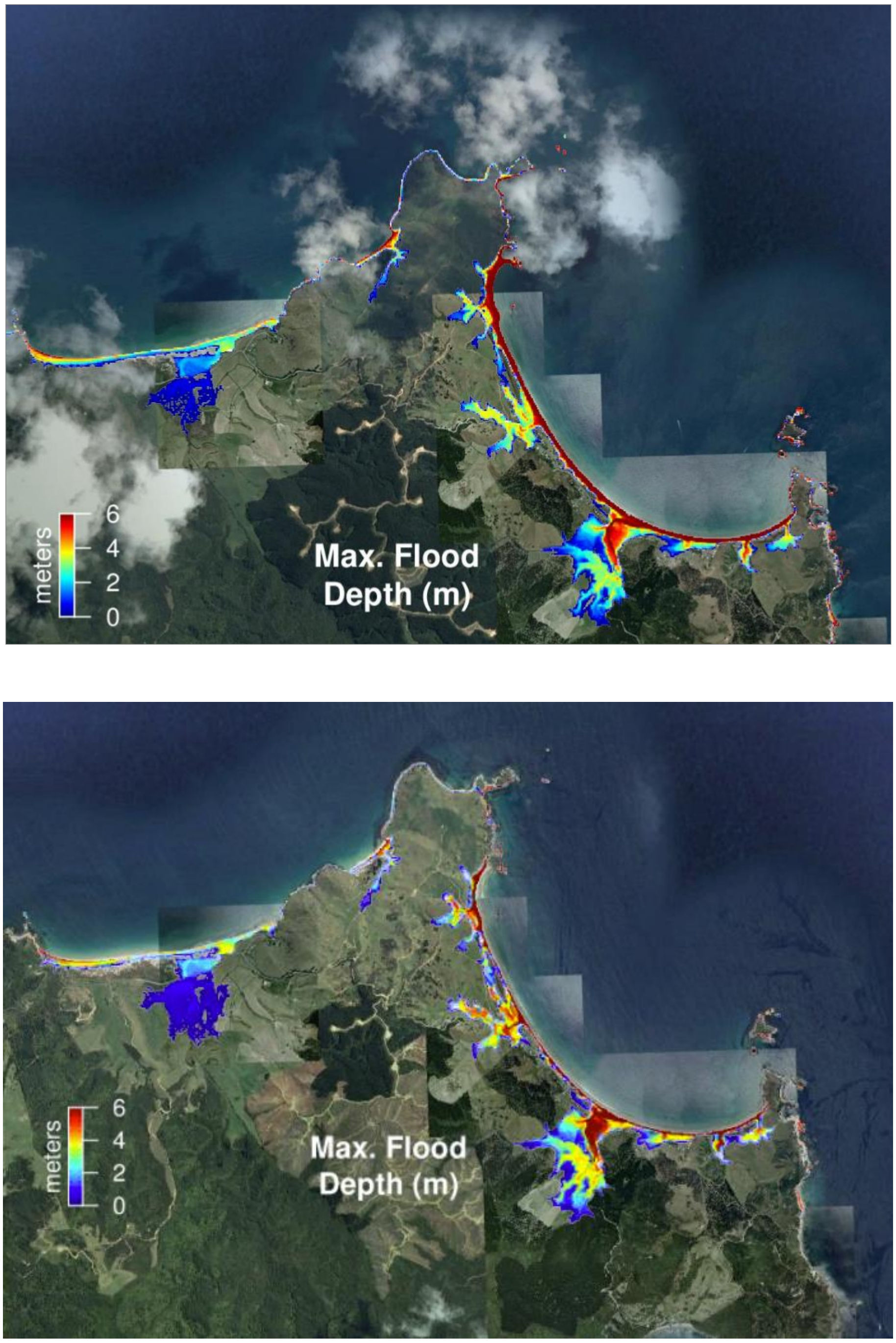

Figure 3.10 Maximum computed tsunami flood depths above ground level at Opito Bay for scenario TK 8 MSL (top) and TK 8 HT (bottom).

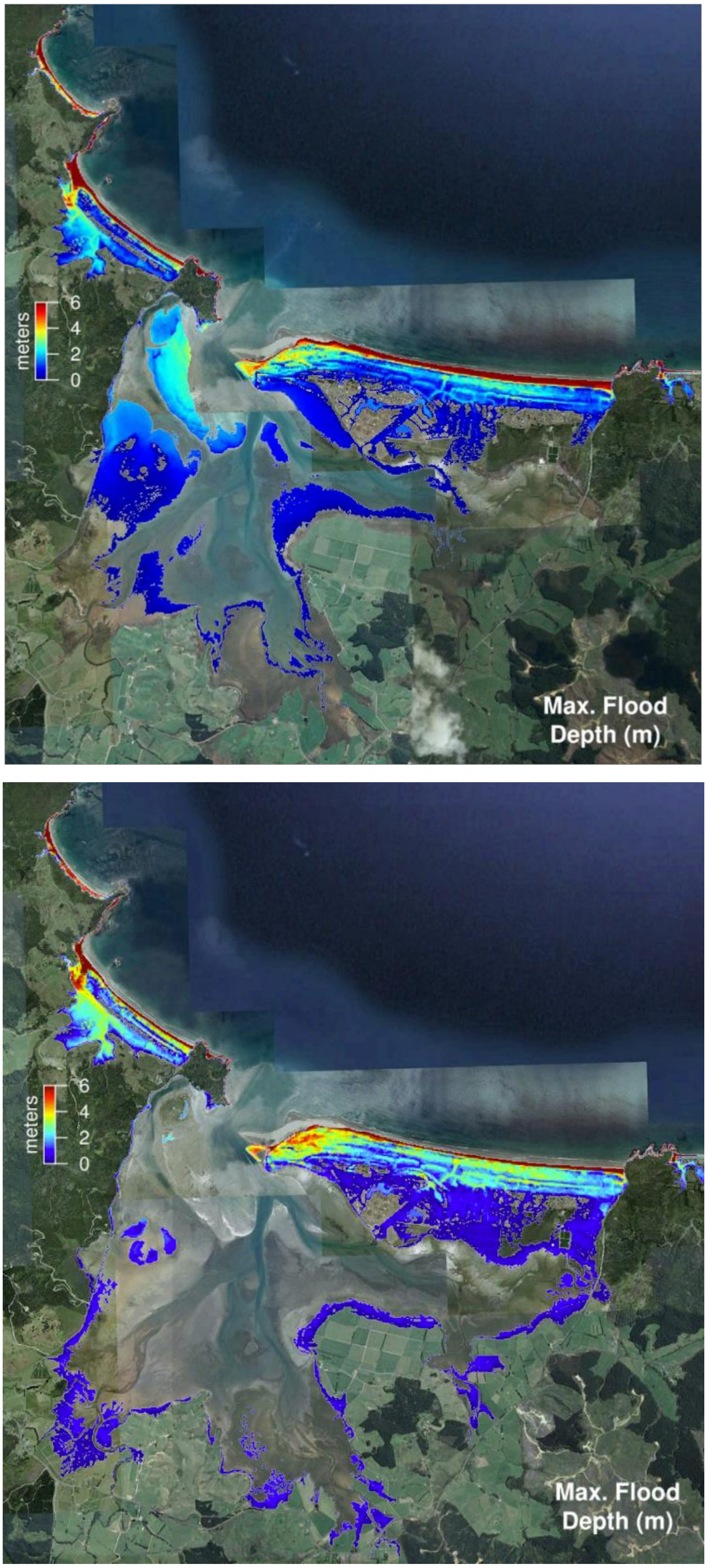

Figure 3.11 Maximum computed tsunami flood depths above ground level at Whangapoua for scenario TK 8 MSL (top) and TK 8 HT (bottom).

3.3 Tsunami Current Speeds

Given the extreme wave heights generated by the TK Trench sources, strong currents would also be expected, particularly through the narrow entrance to Kennedy Bay, Kennedy Bay estuary and Whangapoua estuary. The variations in current speeds at these locations between the least and most severe scenarios (TK 1 and TK 8 respectively) are shown in Figure 3.12.

Perhaps more important than simply knowing the maximum current speed, the duration of strong currents is also important. This concept is illustrated in the time-current-threshold map shown in. In this figure, we choose a particular current speed threshold and plot, as a colour, the time (in hours) over which that threshold is exceeded. In this example, we see that for scenario TK 1, the threshold of 3 knots (~1.5 m/s) is exceeded for the first hour inside the entrance to Whangamata Harbour, while currents exceed this threshold for up to 3 hours just outside the harbour entrance. In the more extreme scenario TK 8, we see that the 5-knot threshold is exceeded for up to 6 hours through the harbour entrance with varying degrees of exceedance throughout the near shore zone.

We emphasize here that this does not mean currents of this threshold are exceeded continuously over the time duration, but rather, that current speed threshold is exceeded at least once in the time span indicated. The full set of time-current-threshold maps is contained in Appendix 4.

Current hazard plots are presented in Figure 3.17. In this figure we simply plot the maximum computed current speed across each source scenario using a banded colour palette. Presented this way, we can see which regions of the model domain are susceptible to what level of currents. The complete set of current hazard zone plots is presented for Whangamata in Appendix 5.

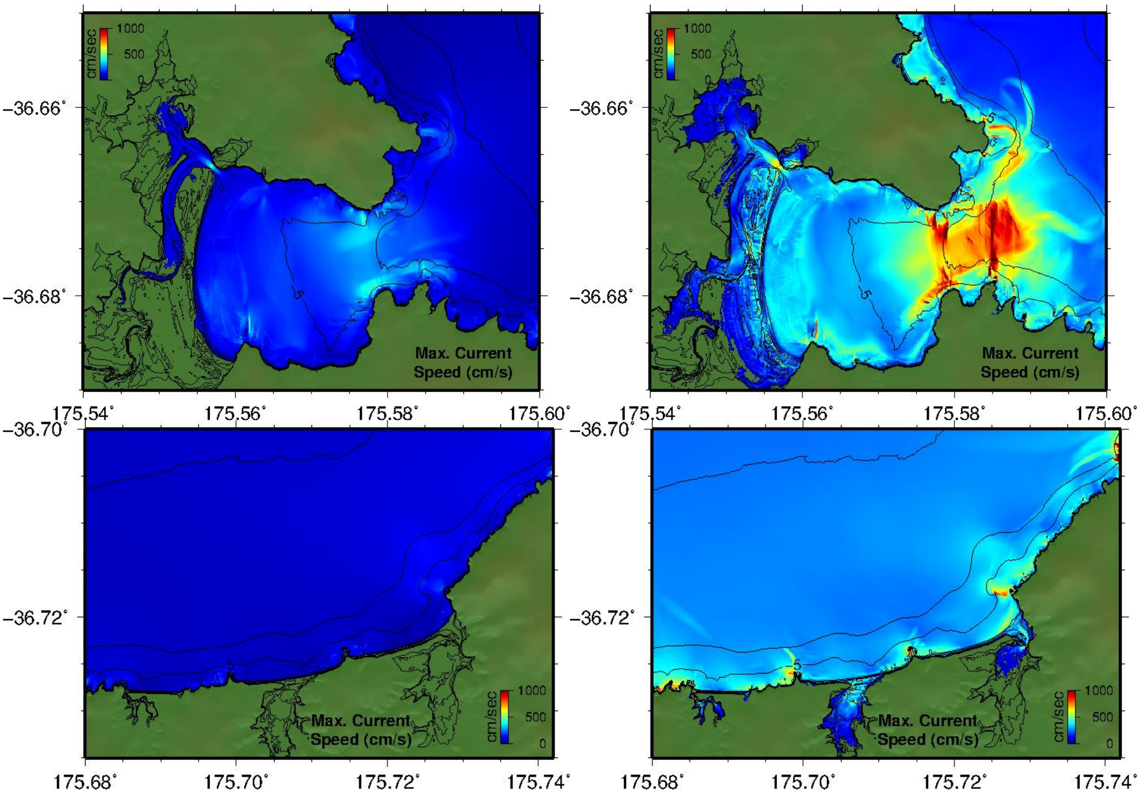

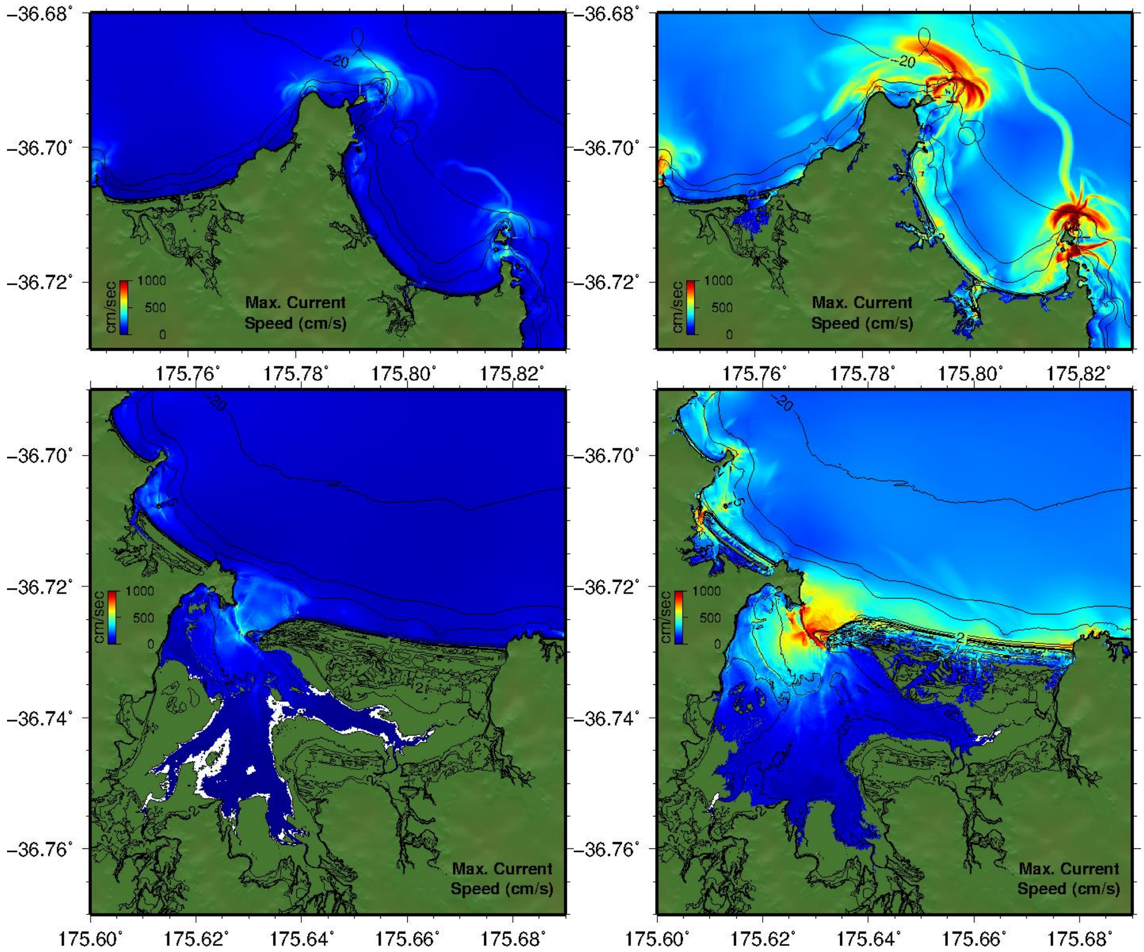

Figure 3.12 Computed maximum current speeds at Kennedy Bay and Whangapoua (previous page, top and bottom respectively) and Opito Bay and Whangapoua (this page, top and bottom respectively) from scenarios TK 1 (left) and TK 8 (right) at MSL.

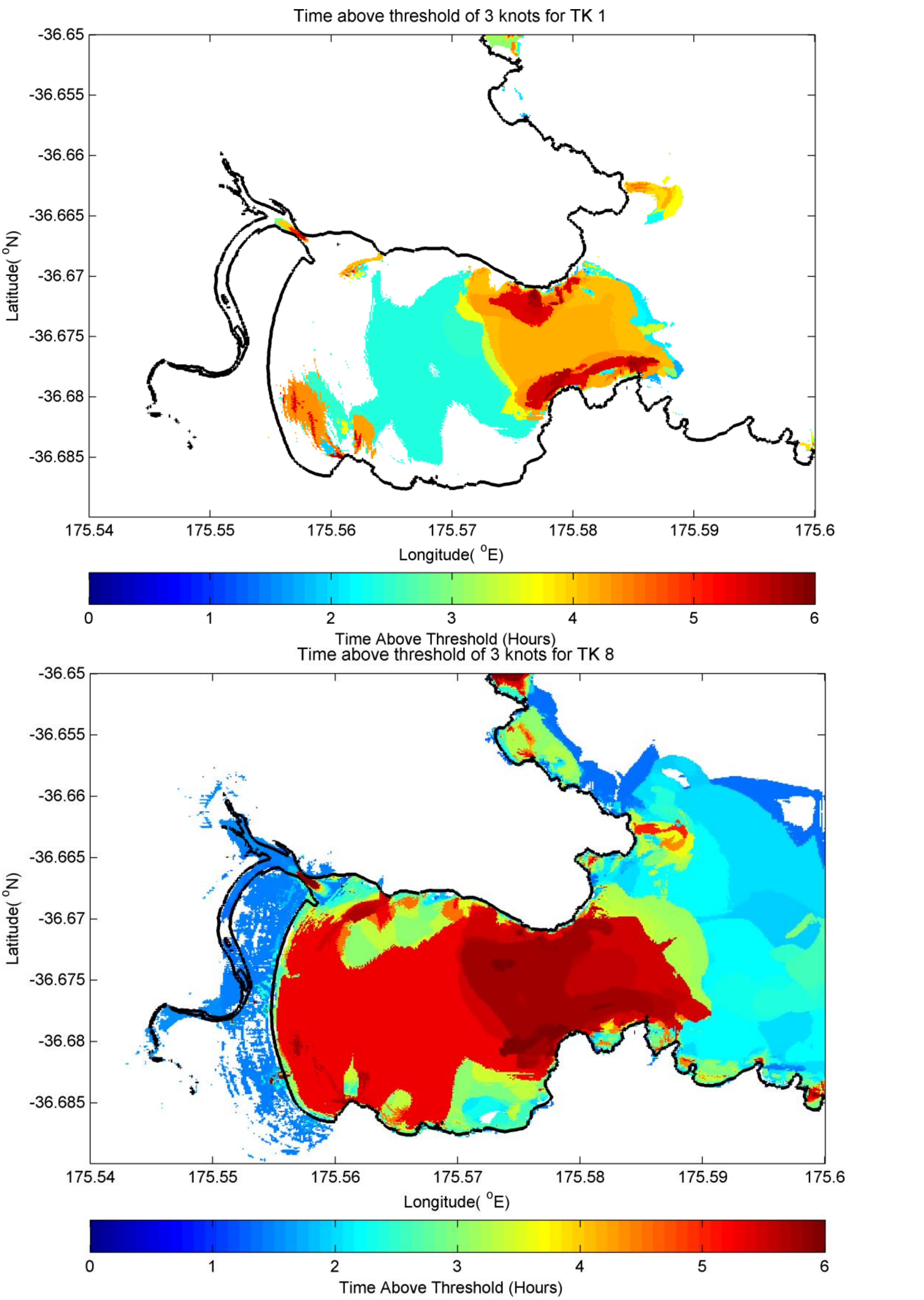

Figure 3.13 Time-current-threshold maps from scenarios TK1 (top) and TK8 (top) at Kennedy Bay.

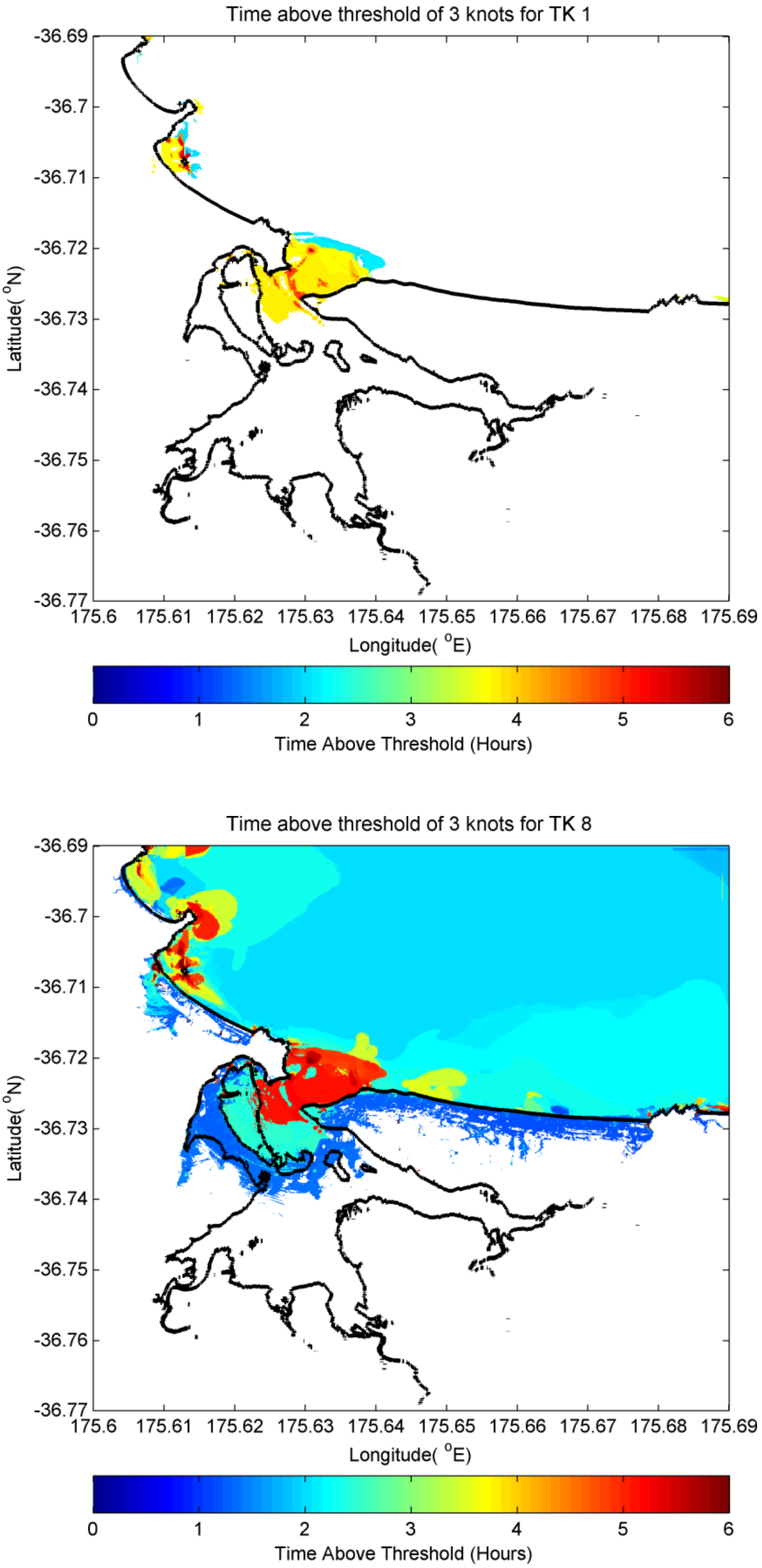

Figure 3.14 Time-current-threshold maps from scenarios TK1 (top) and TK8 (top) at Whangapoua.

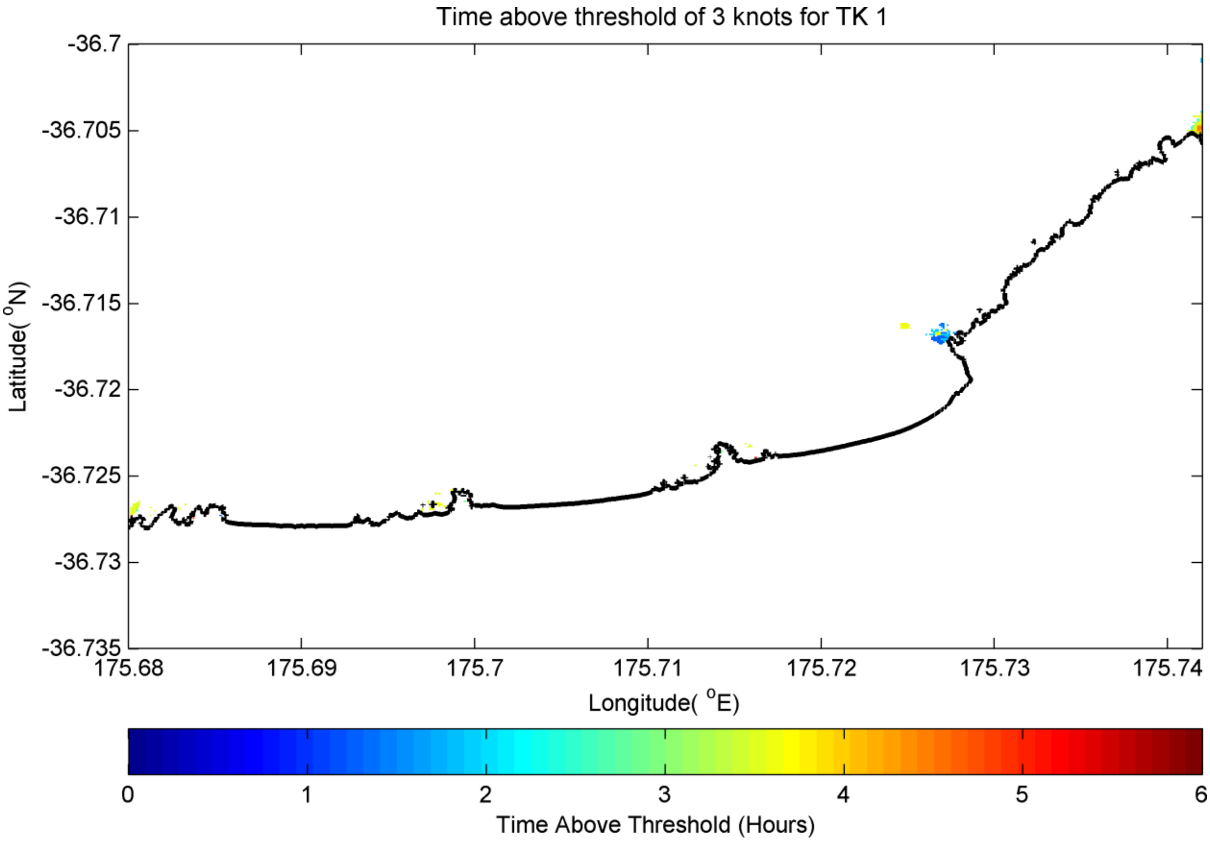

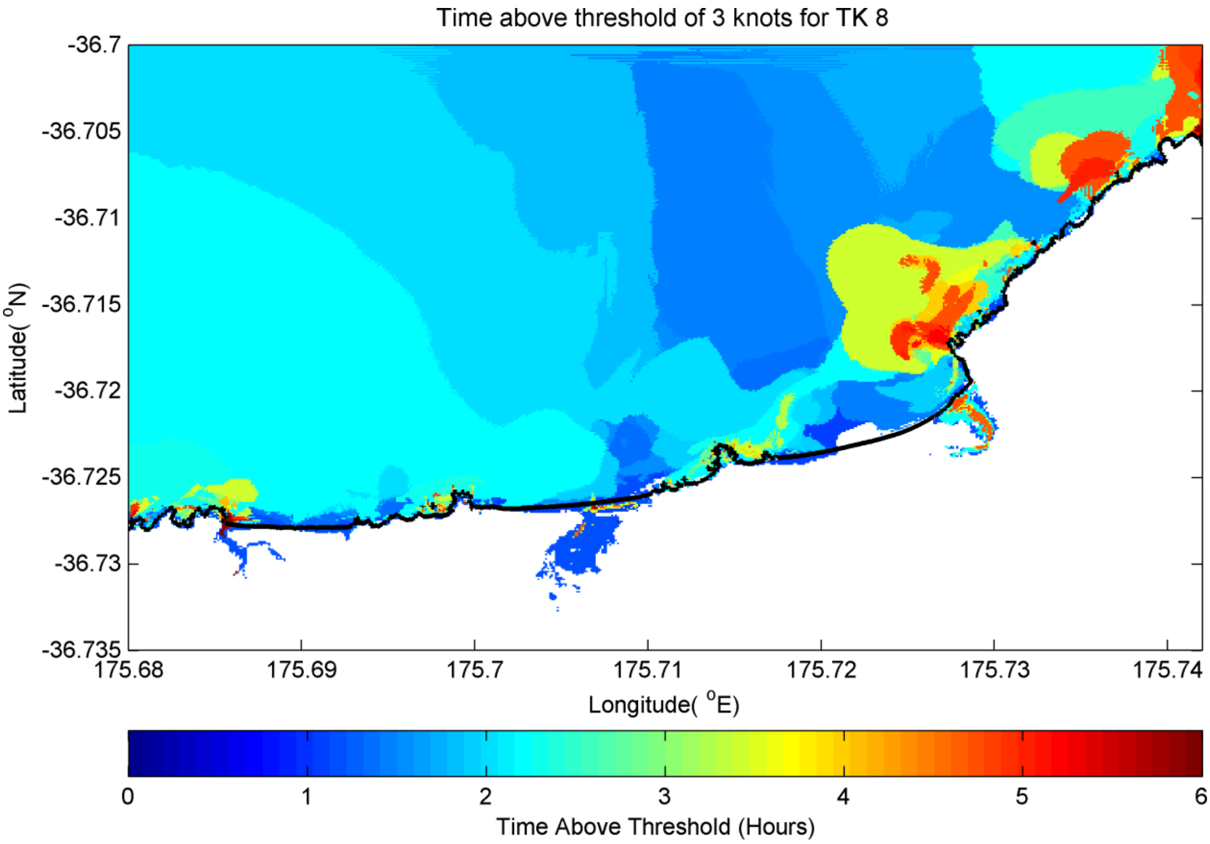

Figure 3.15 Time-current-threshold maps from scenarios TK1 (top) and TK8 (top) at Kuaotunu.

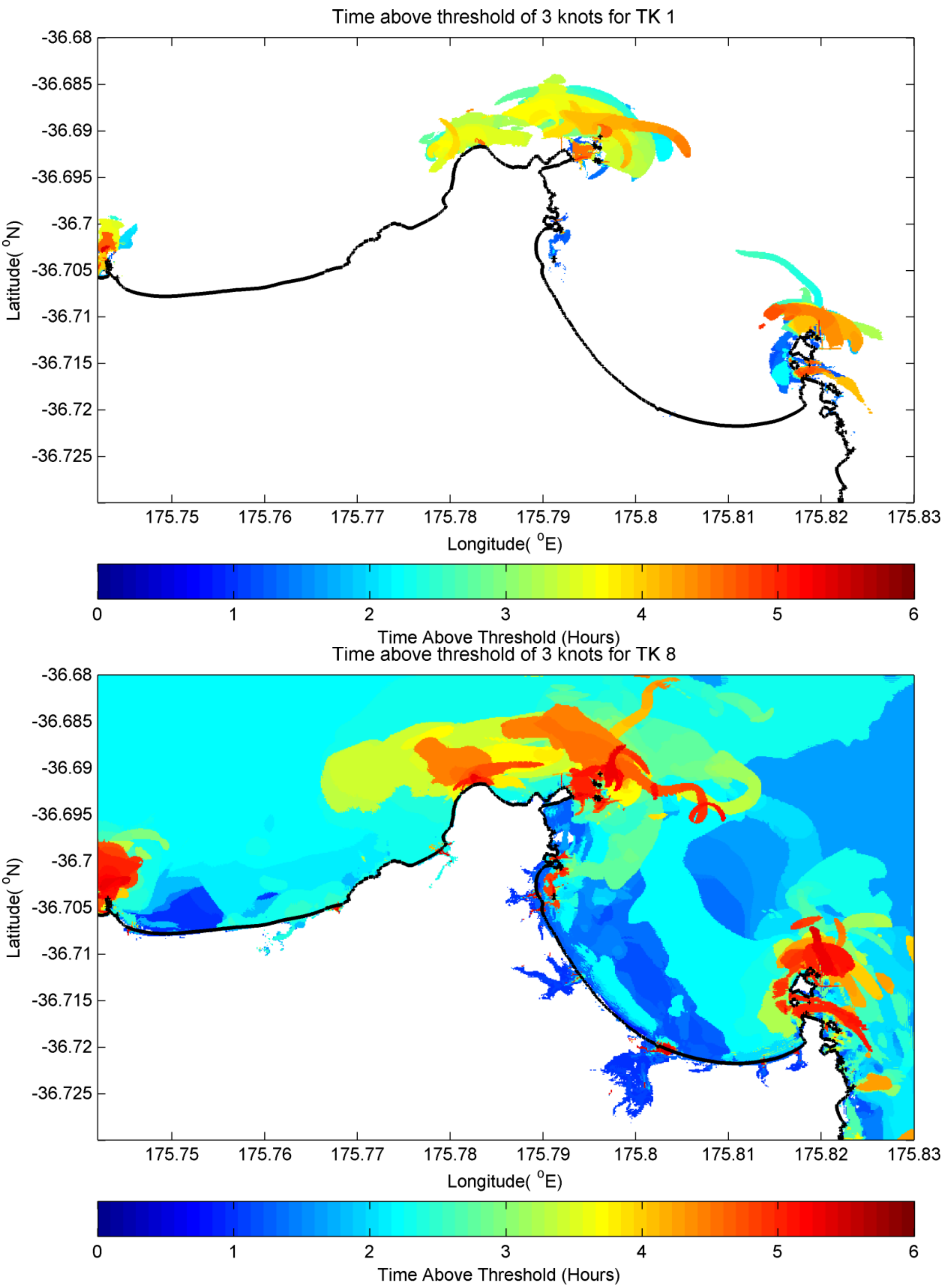

Figure 3.16 Time-current-threshold maps from scenarios TK1 (top) and TK8 (top) at Opito Bay.

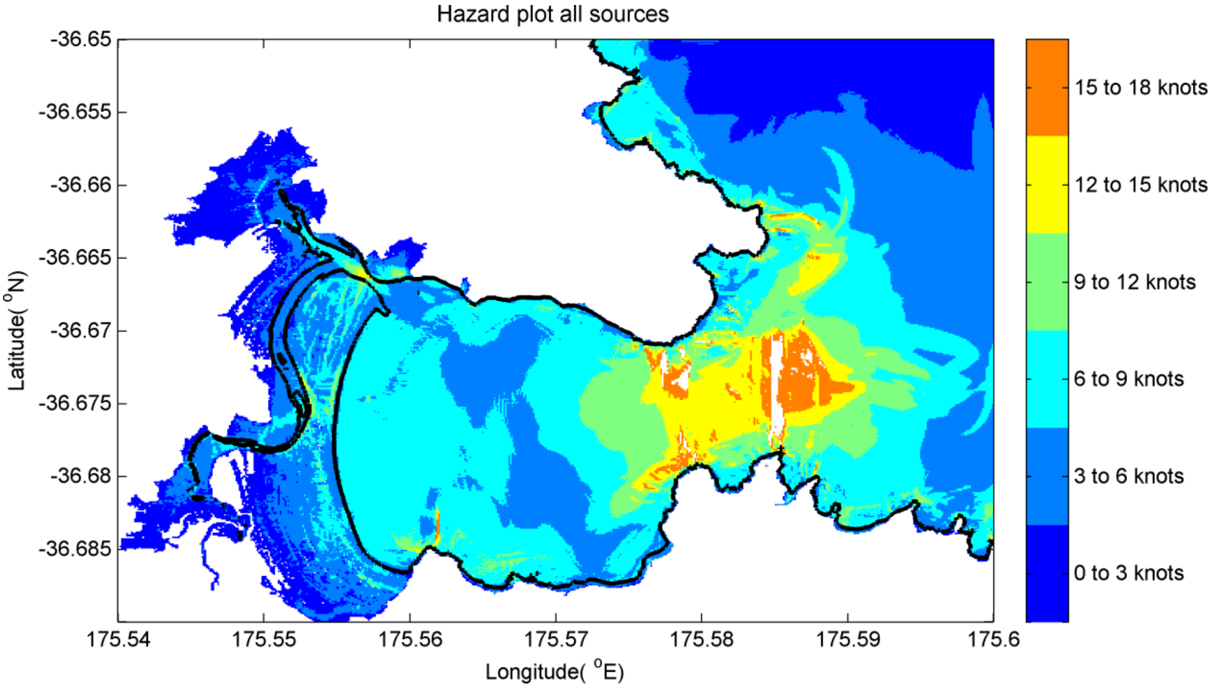
Hazard plot all sources
-36.65
-36.655
-36.66
-36.665
-36.67
-36.675
-36.68
-36.685
Latitude(°N)
175.54
175.55
175.56
175.57
175.58
175.59
175.6
Longitude(°E)
15 to 18 knots
12 to 15 knots
9 to 12 knots
6 to 9 knots
3 to 6 knots
0 to 3 knots

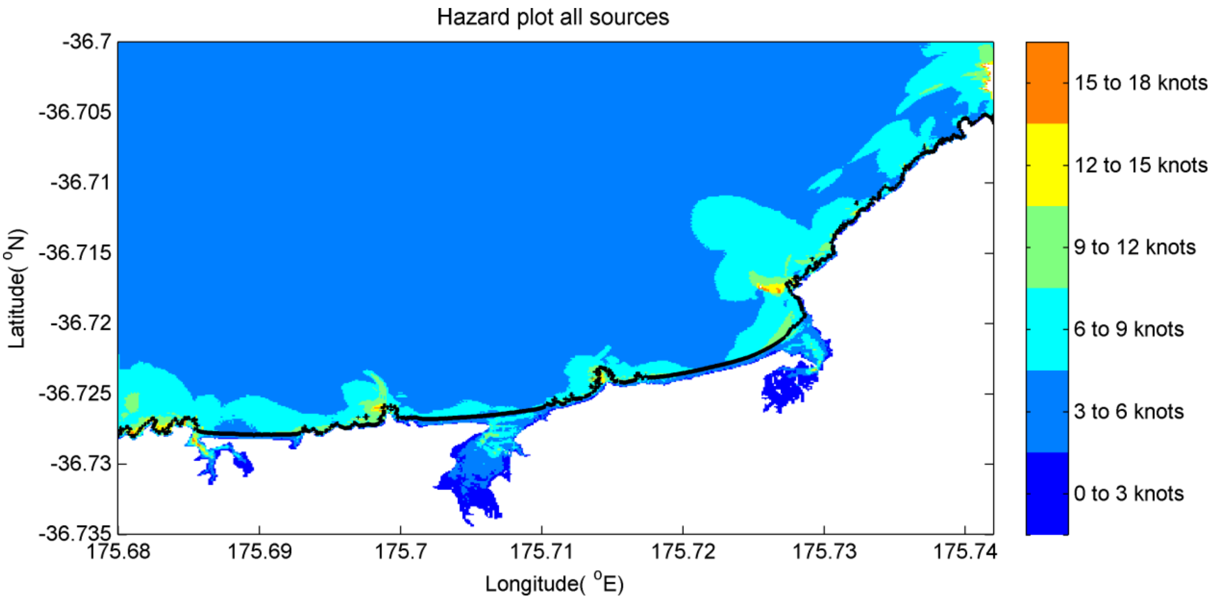
Hazard plot all sources
-36.7
-36.705
-36.71
-36.715
-36.72
-36.725
-36.73
-36.735
Latitude(°N)
175.68
175.69
175.7
175.71
175.72
175.73
175.74
Longitude(°E)
15 to 18 knots
12 to 15 knots
9 to 12 knots
6 to 9 knots
3 to 6 knots
0 to 3 knots

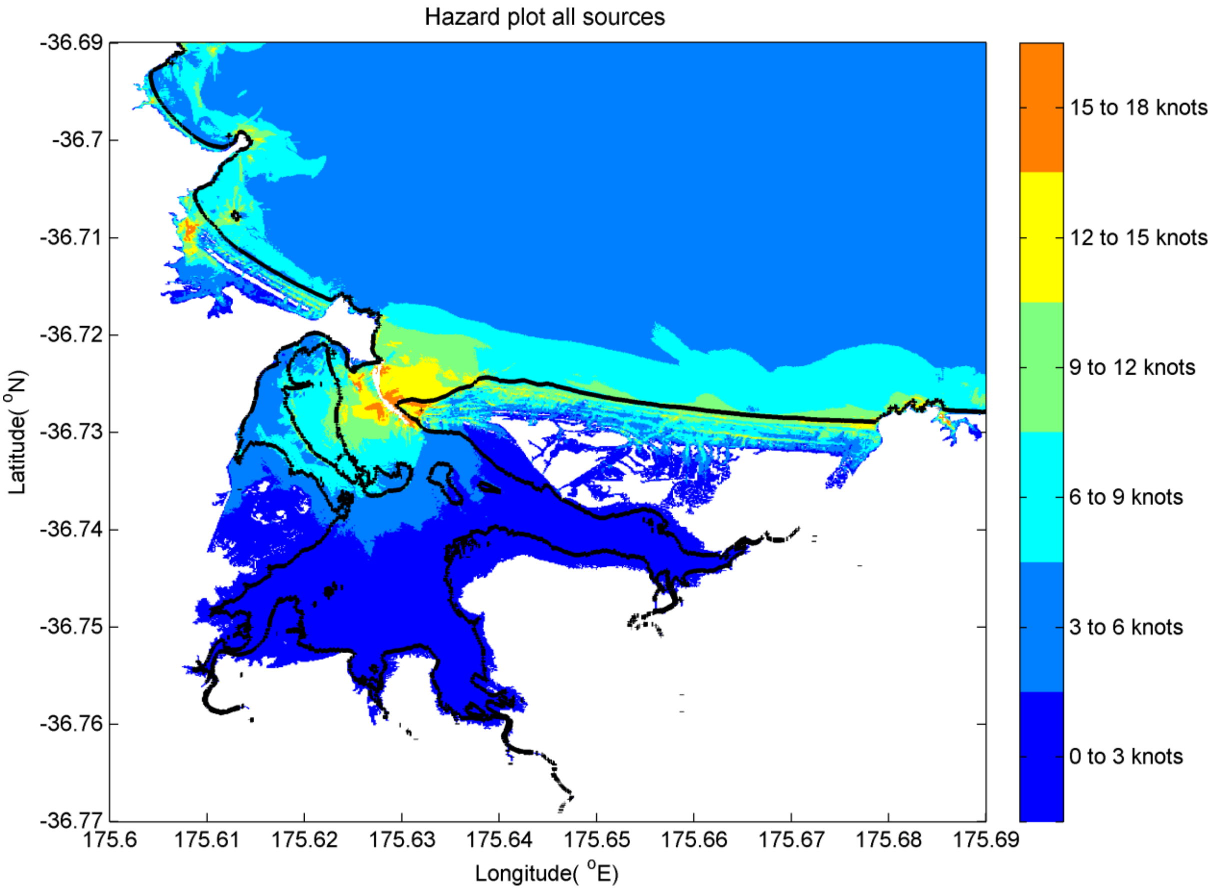

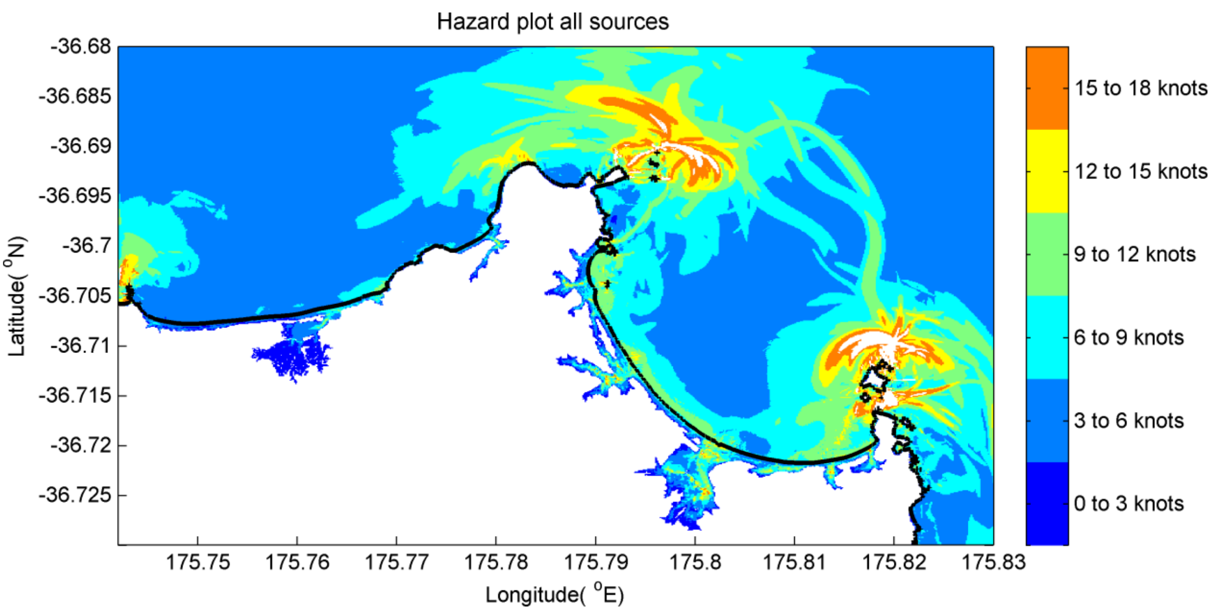

Figure 3.17 (above and previous page) Current hazard zones for the four C grid regions.

4 MODEL RESULTS: DISTANT SOURCE TSUNAMIS

4.1 Propagation models

Tsunami inundation, water levels and current speeds for the sources described in Section 2.2 above were modelled at Kennedy Bay, Whangapoua, Kuaotunu and Opito Bay. For each of the cases, we have plotted the modelled trans-Pacific tsunami wave heights and the modelled wave heights closer to New Zealand. As shown in Figure 4.1 there is a wide discrepancy in the wave heights between sources with widely disparate magnitudes, i.e. source FF1, the 1960 Valdivia earthquake (M9.5) and source FF2, the 2010 Maule event (M8.8). In Figure 4.2, you can see the different propagation patterns between sources with similar magnitudes located in different areas. It is clear that sources located in the Peru/Chile border region (Chile North 2&3 – FF5 and FF6) transmit more tsunami wave energy towards New Zealand than the source located further to the south (Chile North 1, FF4).

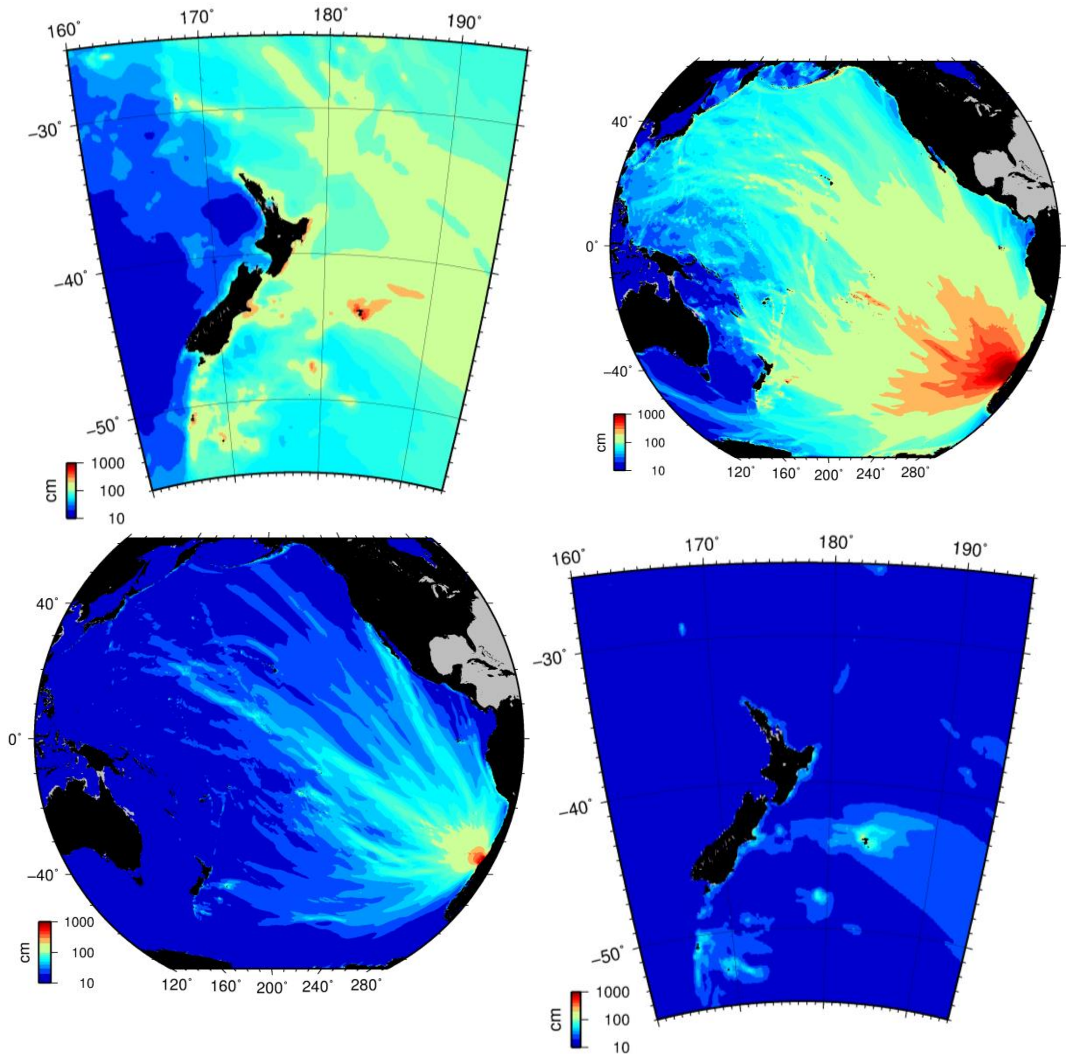

Figure 4.1 Comparison between trans-Pacific propagation patterns for the 1960 Valdivia, Chile (top) and 2010 Maule Chile (bottom) tsunamis.

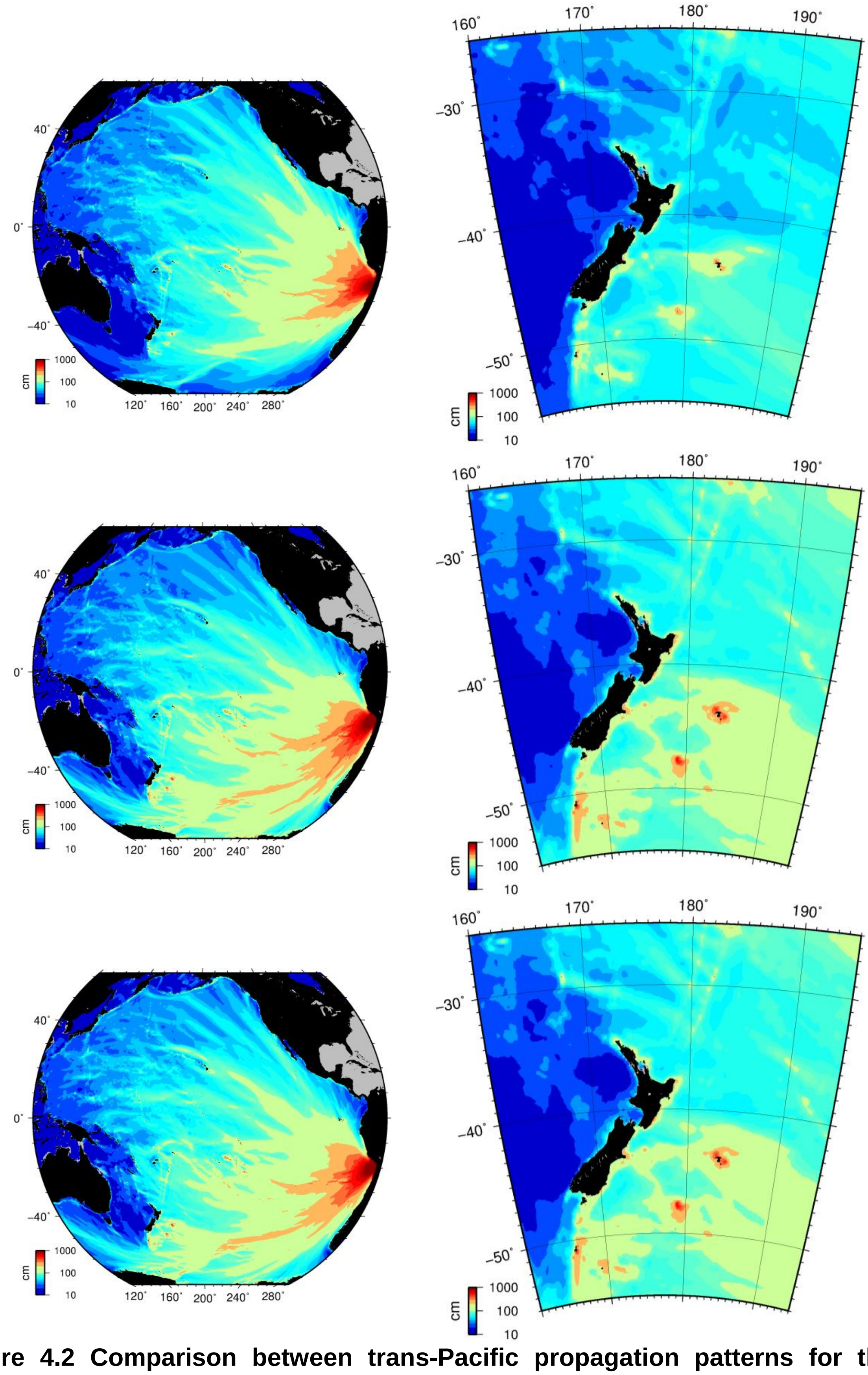

Figure 4.2 Comparison between trans-Pacific propagation patterns for the three hypothetical northern Chile scenarios: Chile North 1 (top) Chile North 2 (mid) and Chile North 3 (bottom).

4.2 Arrival Times

Modelled time series of water level from a nearshore point at each location for each of the distant source cases is presented in Figure 4.3 through Figure 4.6. Variations in the timing and character of the modelled tsunami waves are evident. We note that sources in southern Chile arrive earlier than do sources located further north. It is also important to note that the largest wave height generally occurs several hours after tsunami arrival, in direct contrast to the regional sources.

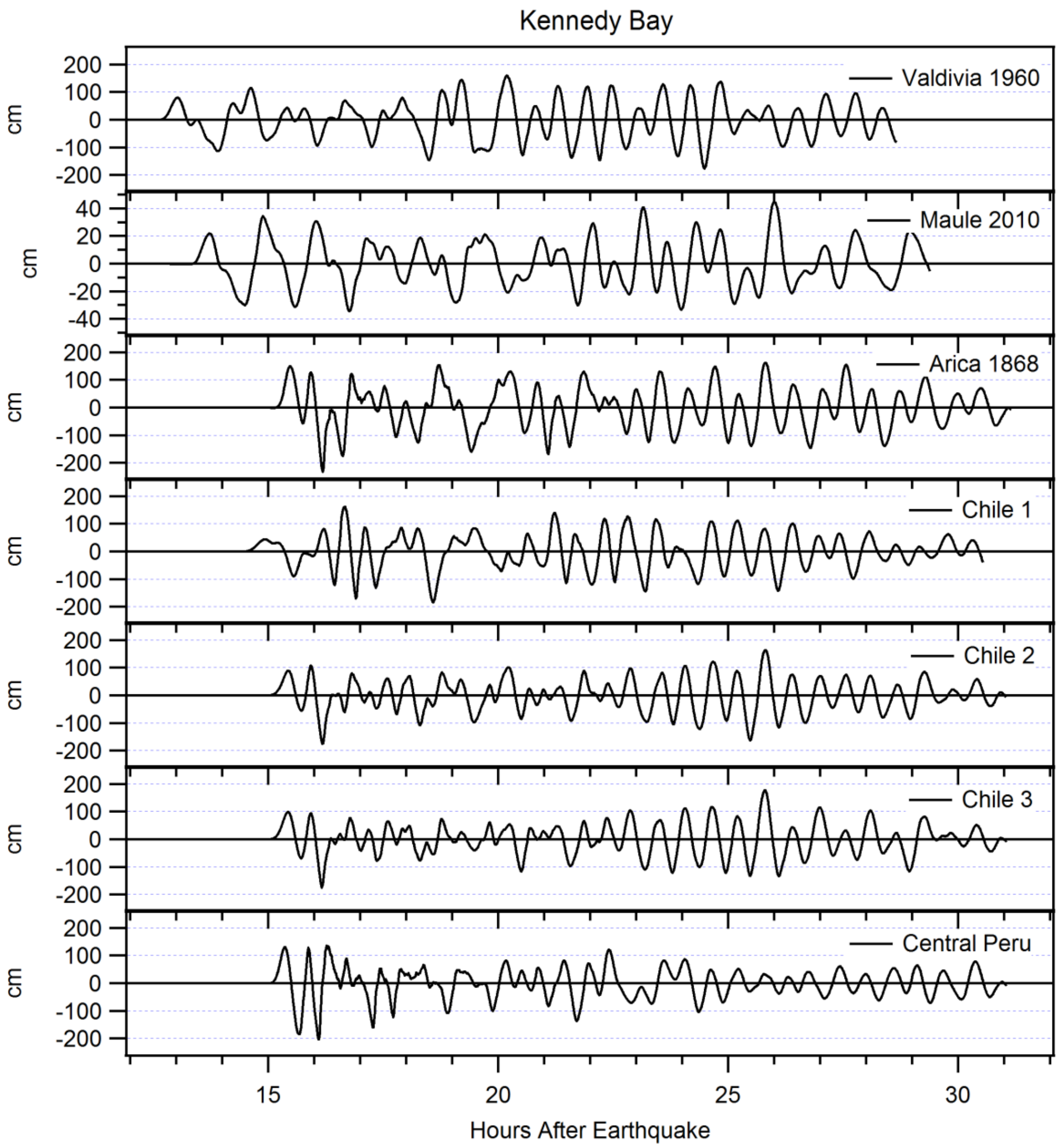

Figure 4.3 Modelled time series of water levels in Kennedy Bay for each of the distant source scenarios. Note the different scale for the Chile 2010 case.

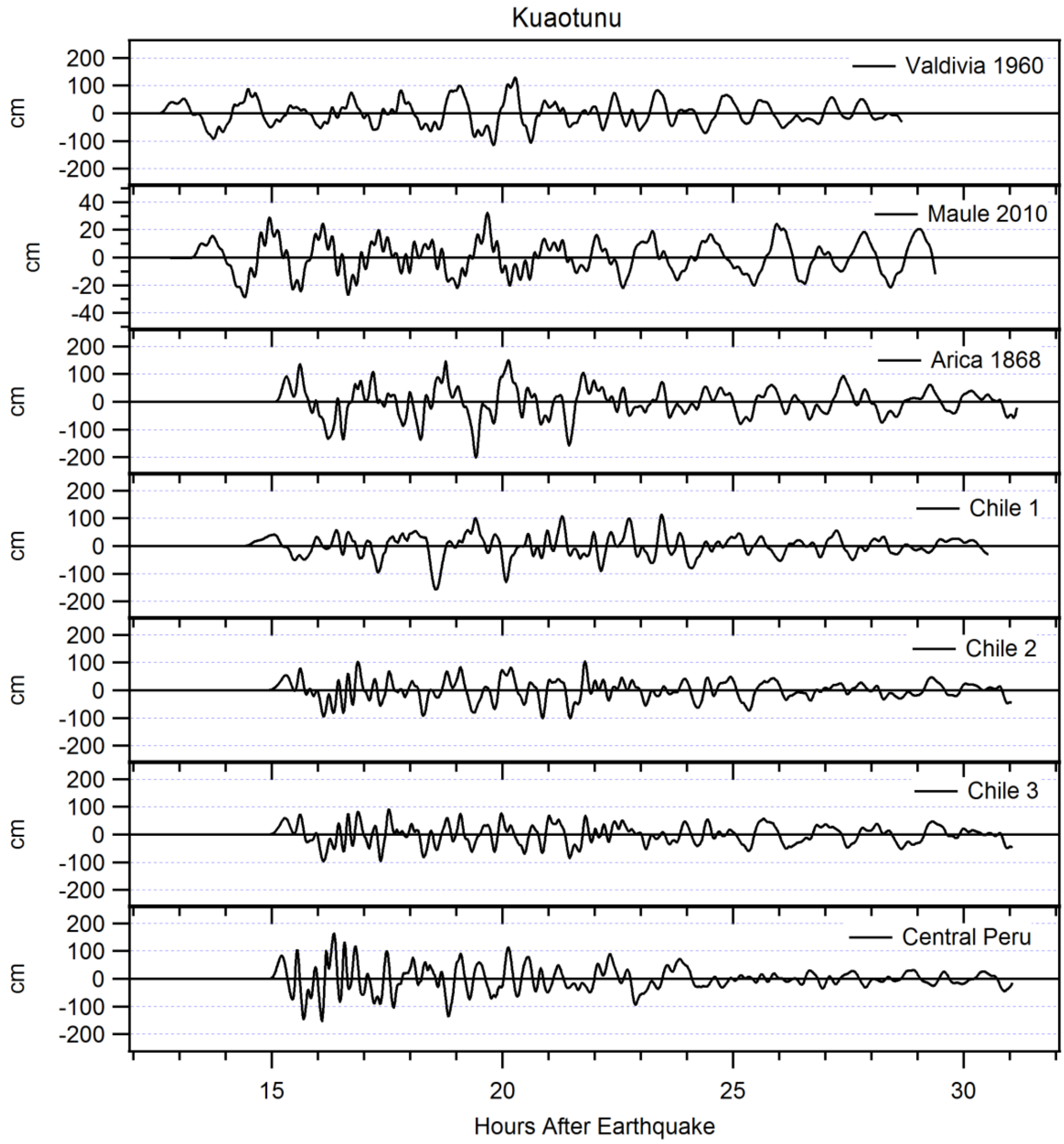

Figure 4.4 Modelled time series of water level at Kuaotunu for each of the distant source scenarios. Note the different scale for the Chile 2010 case.

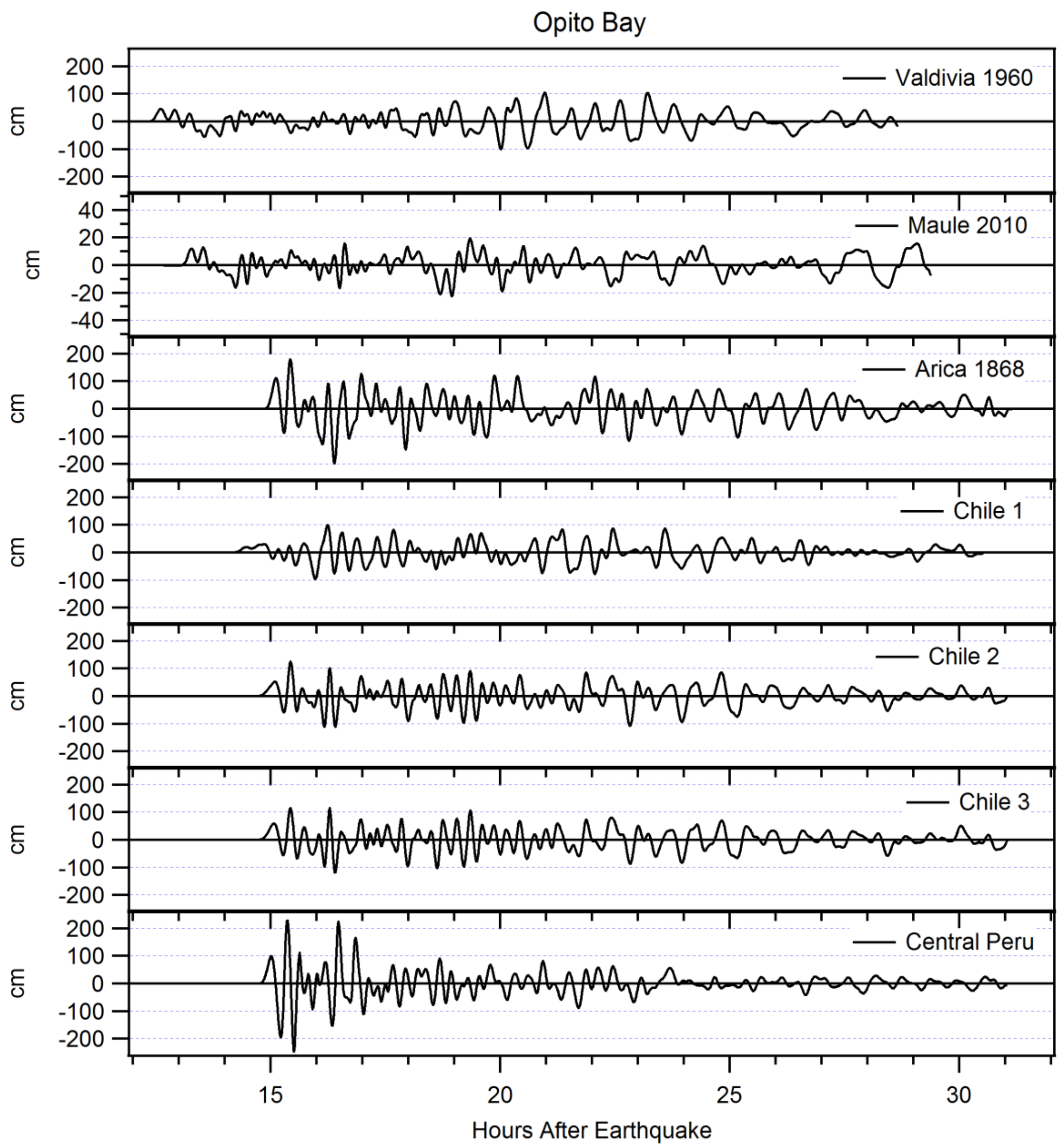

Figure 4.5 Modelled time series of water levels in Opito Bay for each of the distant source scenarios. Note the different scale for the Chile 2010 case.

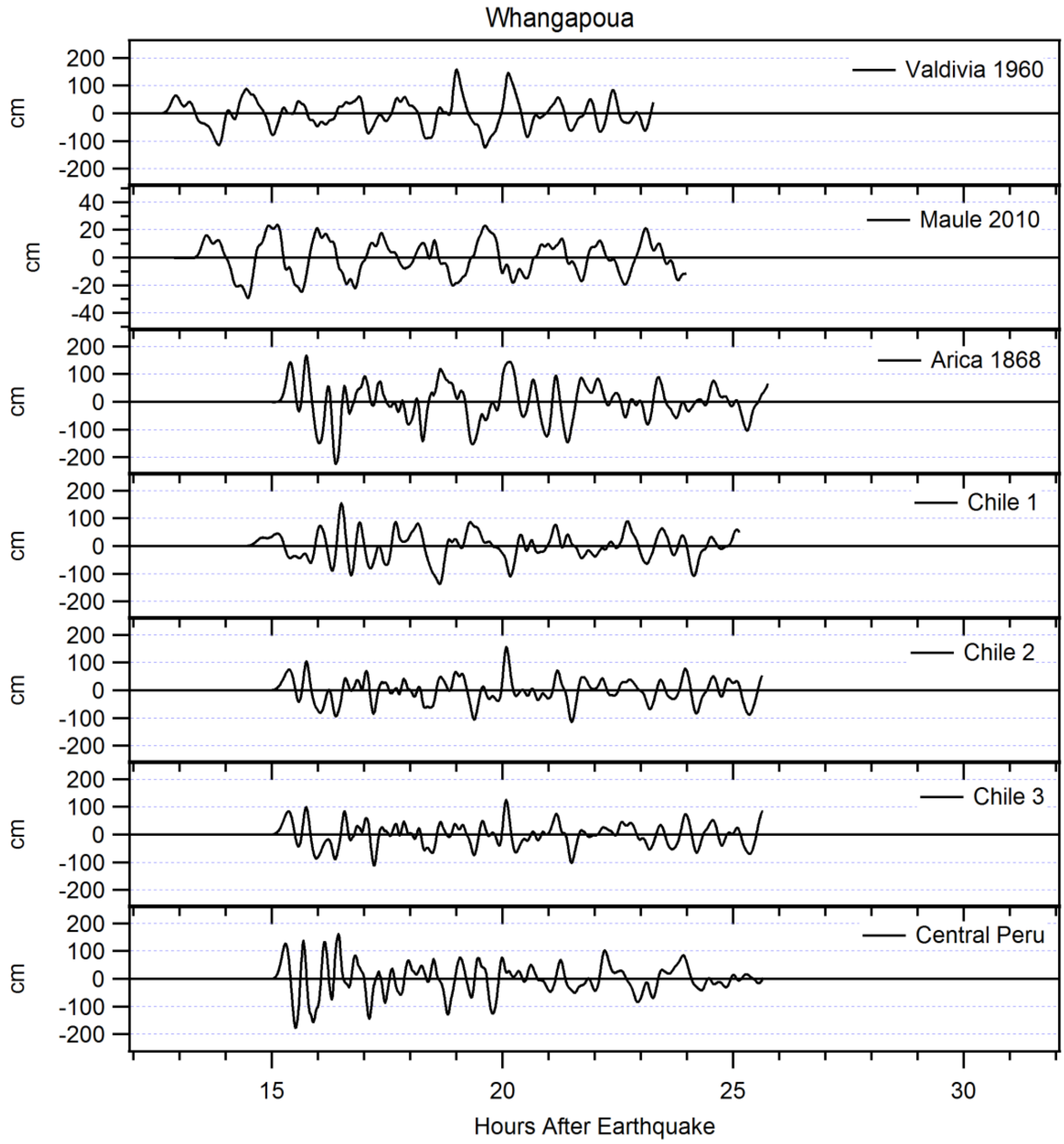

Figure 4.6 Modelled time series of water levels at Whangapoua for each of the distant source scenarios. Note the different scale for the Chile 2010 case.

4.3 Tsunami Height

Modelled tsunami heights from the distant source scenarios for Kennedy Bay, Kuaotunu, Opito Bay and Whangapoua are plotted in the following figures (a complete set of the model results is contained in the Appendices). In Figure 4.7 we compare the results from the 1960 Valdivia source to the 2010 Maule Source, it is clear that the 1960 scenario produced much larger wave heights than 2010, consistent with historical accounts.

In Figure 4.8 we compare the model results between the 1868 Arica scenario and the Chile North 1 scenario. In this comparison, it is evident that these scenarios produce comparable tsunami heights at Kennedy Bay and Whangapoua however at Kuaotunu and Opito Bay, the Arica 1868 results are noticeably larger. The output from the distant source propagation results, shown in Figure 4.9, clearly indicate that the Arica 3 scenario overall produces larger wave heights around New Zealand.

None of the scenarios modelled produced significant overland inundation. While the tsunami surges at Kennedy Bay and Whangapoua enter the respective harbours producing strong currents (discussed in the next section), the only inundation occurs at the stream entrances at the south end of Kennedy Bay beach and in Opito Bay township.

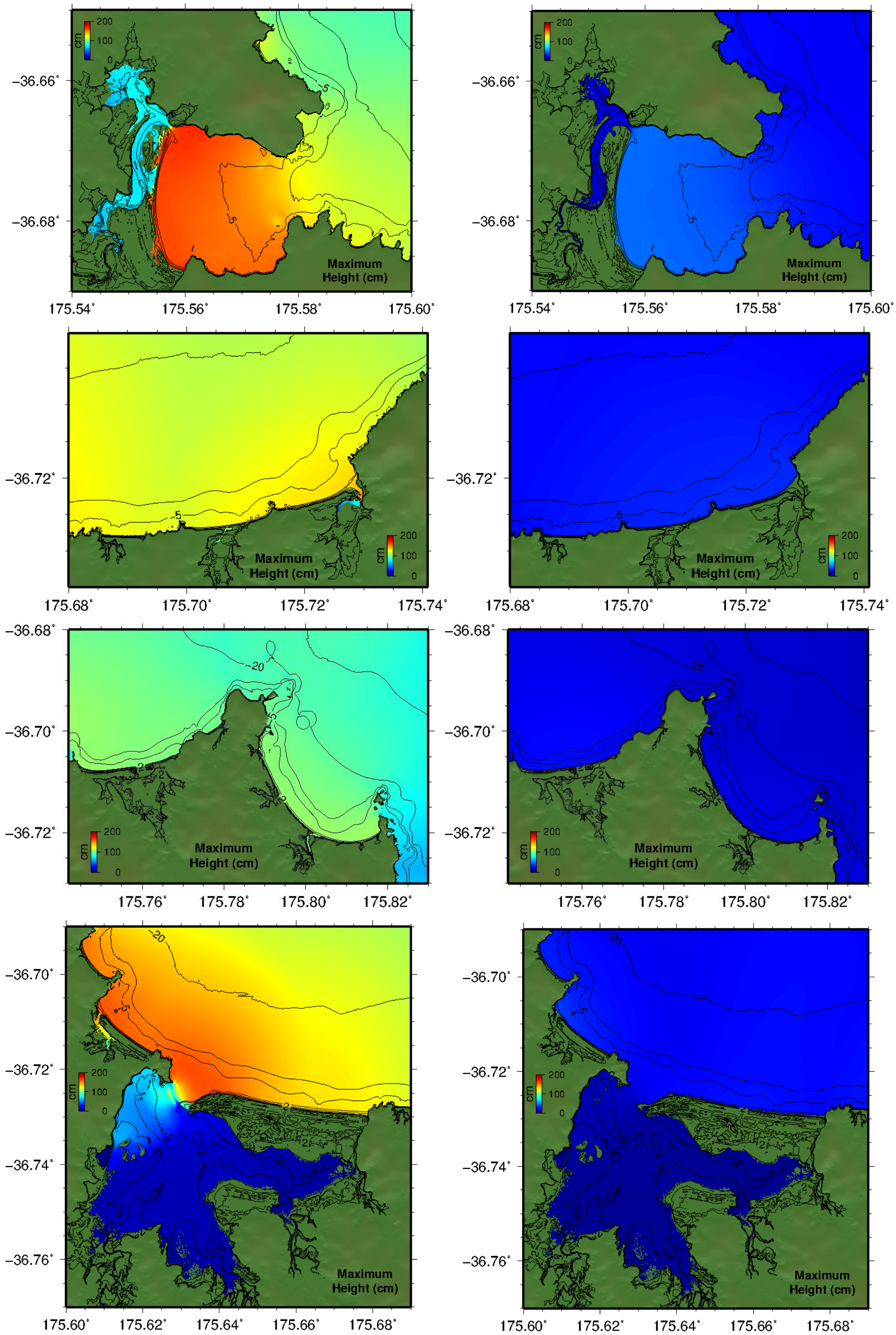

Figure 4.7 Modelled tsunami heights from the 1960 Valdivia scenario (left) and the 2010 Maule Chile scenario (right) for Kennedy Bay, Whangapoua, Kuaotunu and Opito Bay (top to bottom respectively); each case run at HT.

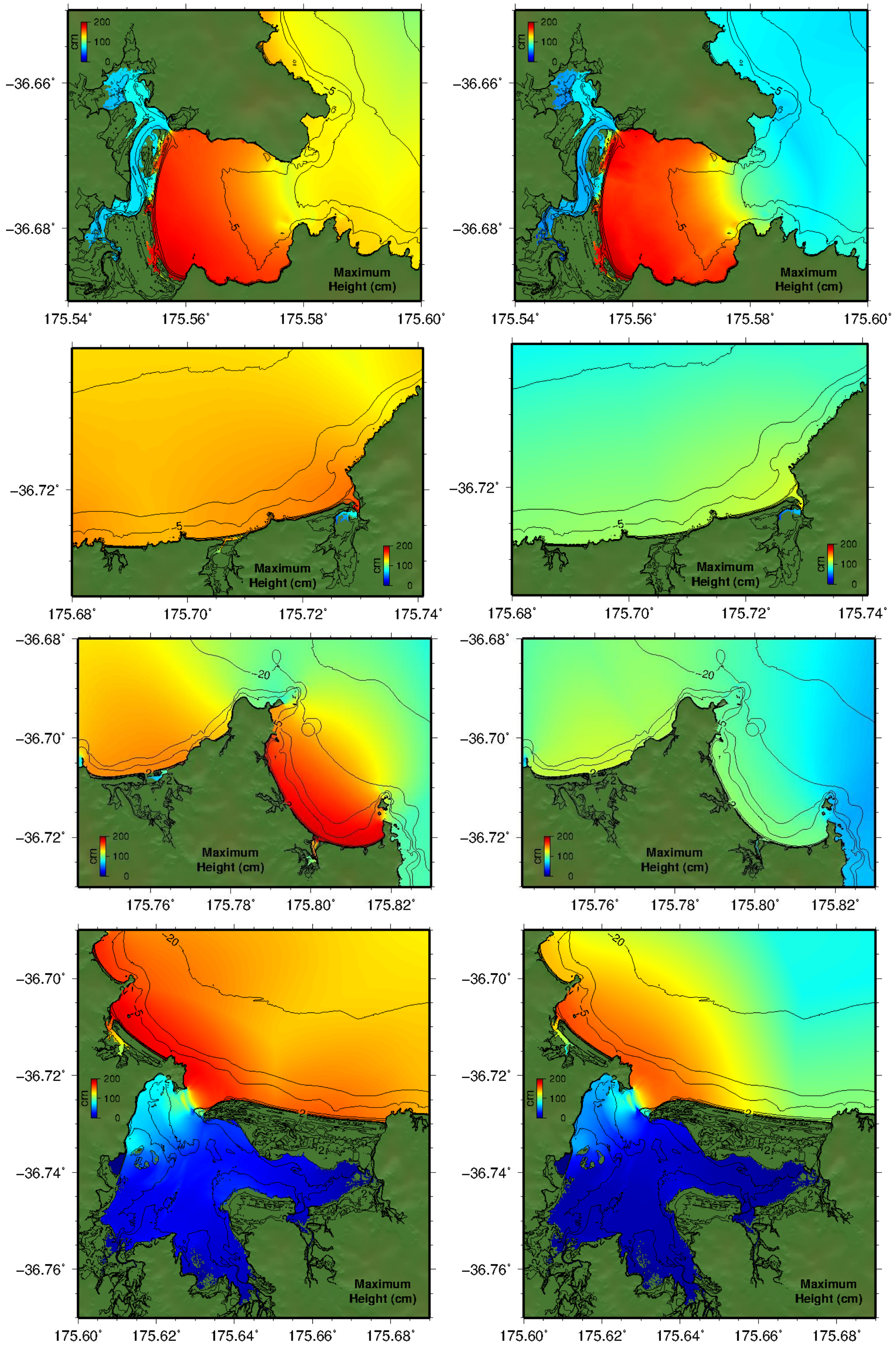

Figure 4.8 Modelled tsunami heights from the 1868 Arica scenario (left) and the Chile North 1 scenario (right) for Kennedy Bay, Whangapoua, Kuaotunu and Opito Bay (top to bottom); each case run at HT.

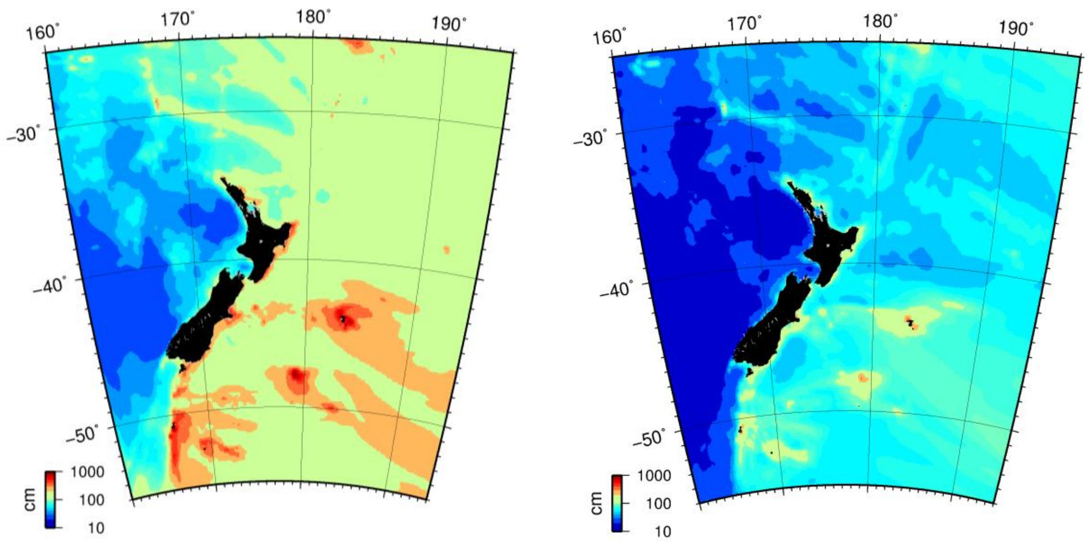

Figure 4.9 Modelled tsunami heights from the propagation model for the 1868 Arica scenario (left) and the Chile North 1 scenario (right).

4.4 Tsunami Current Speeds

As with the TK Trench scenarios, we consider both maximum current speed as well as the duration of these currents. For the distant source scenarios, the duration of strong currents is more important than in the near source cases since the largest tsunami heights occur later in the tsunami time series. In terms of the maximum current speeds, the results from the two largest scenarios, Arica 1868 and Central Peru, are shown in Figure 4.10. We see that the maximum current speeds are of the order of 5 m/s (~10 knots) and occur primarily at the entrance to Kennedy Bay, Kennedy Bay estuary, Whangapoua estuary and in the channels between offshore islands at Opito Bay. Without similar geographical features, the currents at Kuaotunu are much smaller.

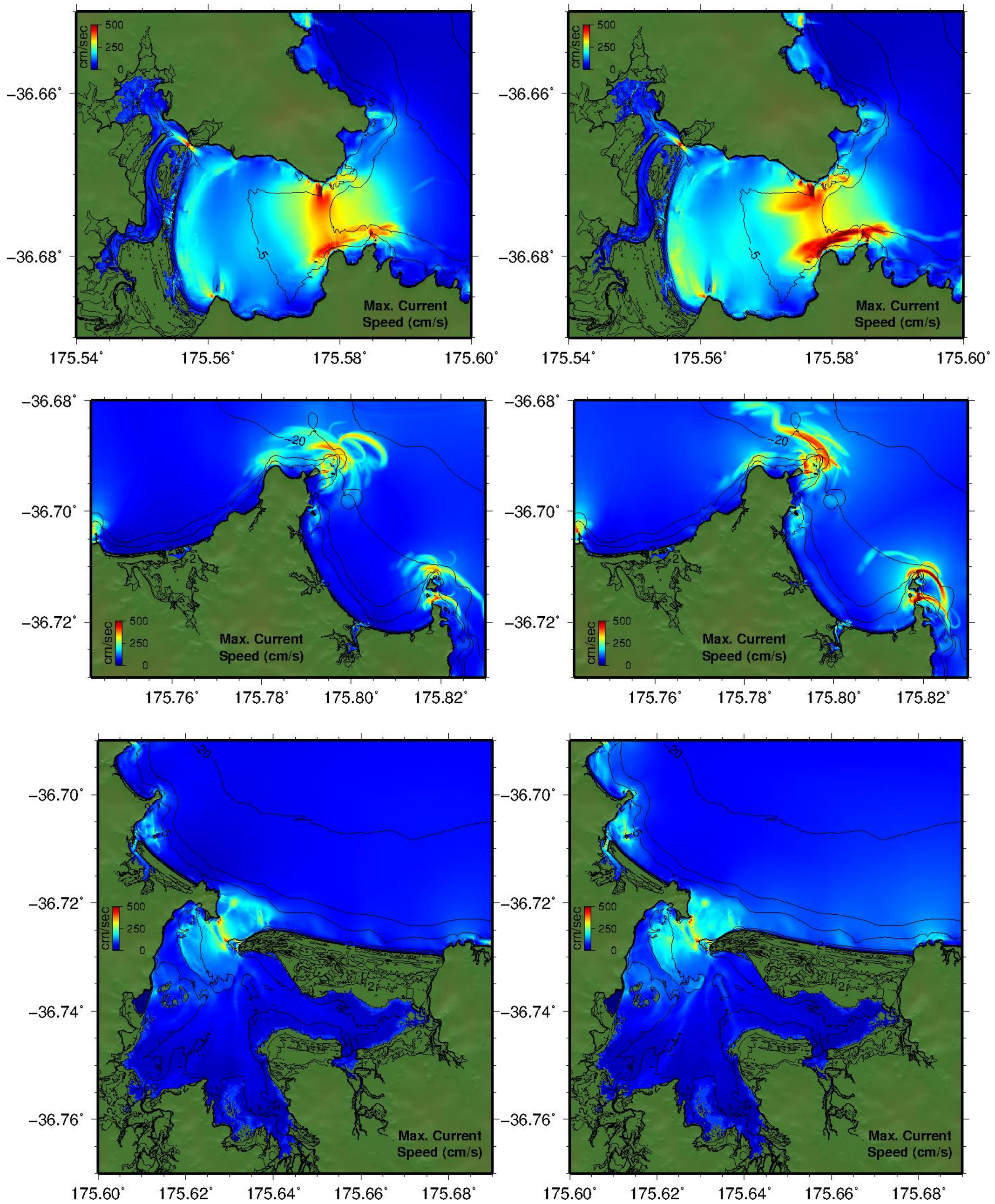

Figure 4.10 Maximum modelled current speeds from the Arica 1868 (left) and Central Peru (right) scenarios for Kennedy Bay, Whangapoua and Opito Bay (top to bottom respectively); each case run at HT.

In terms of the current duration, the plots in Figure 4.11 through Figure 4.14 suggest that current speeds greater than 2 knots would persist at the entrance to Whangamata Harbour and between the Islands for up to 16 hours after tsunami arrival. Finally in, Figure 4.15 the high current speed hazard zones are defined across all distant source tsunami scenarios tested in this study.

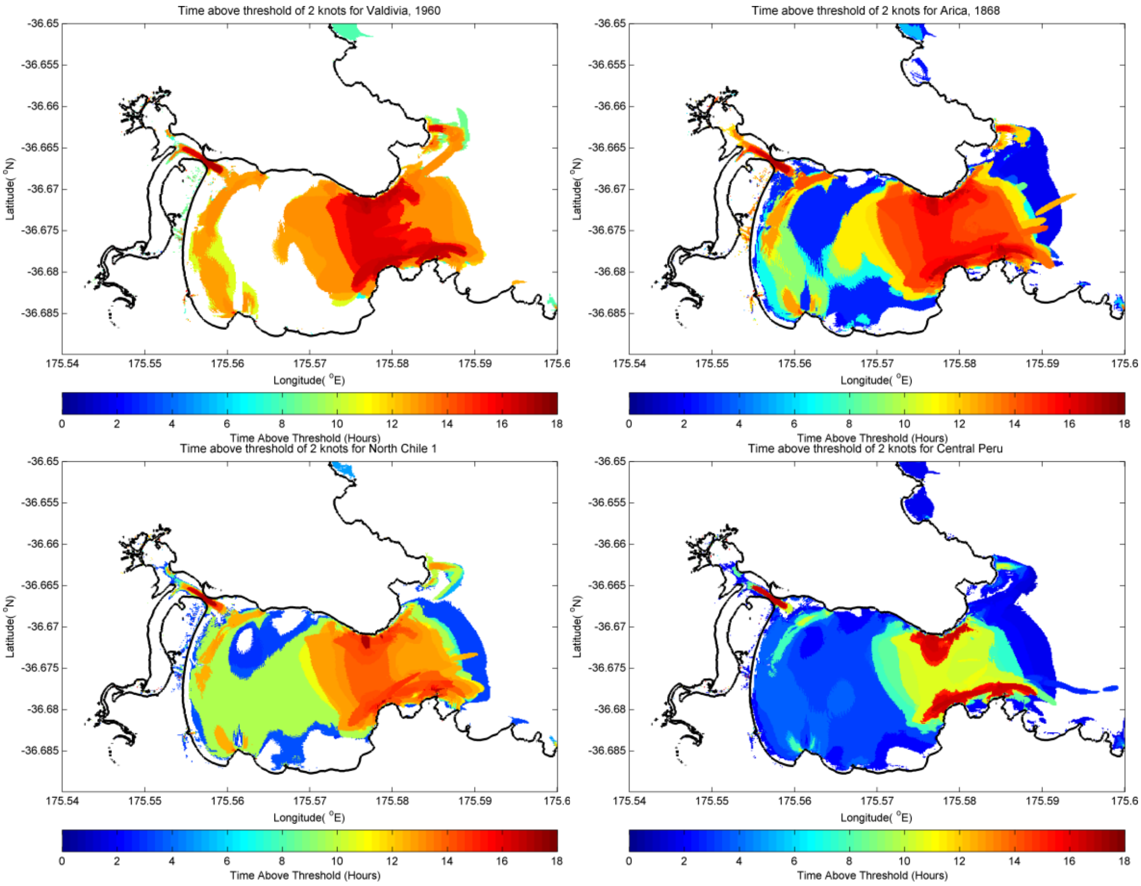

Figure 4.11 Time Current threshold maps for current speeds of 2 knots for the Chile 1960 (top left) Arica 1868 (top right), Chile North 1 (bottom left) and Central Peru (bottom right) at High tide in Kennedy Bay.

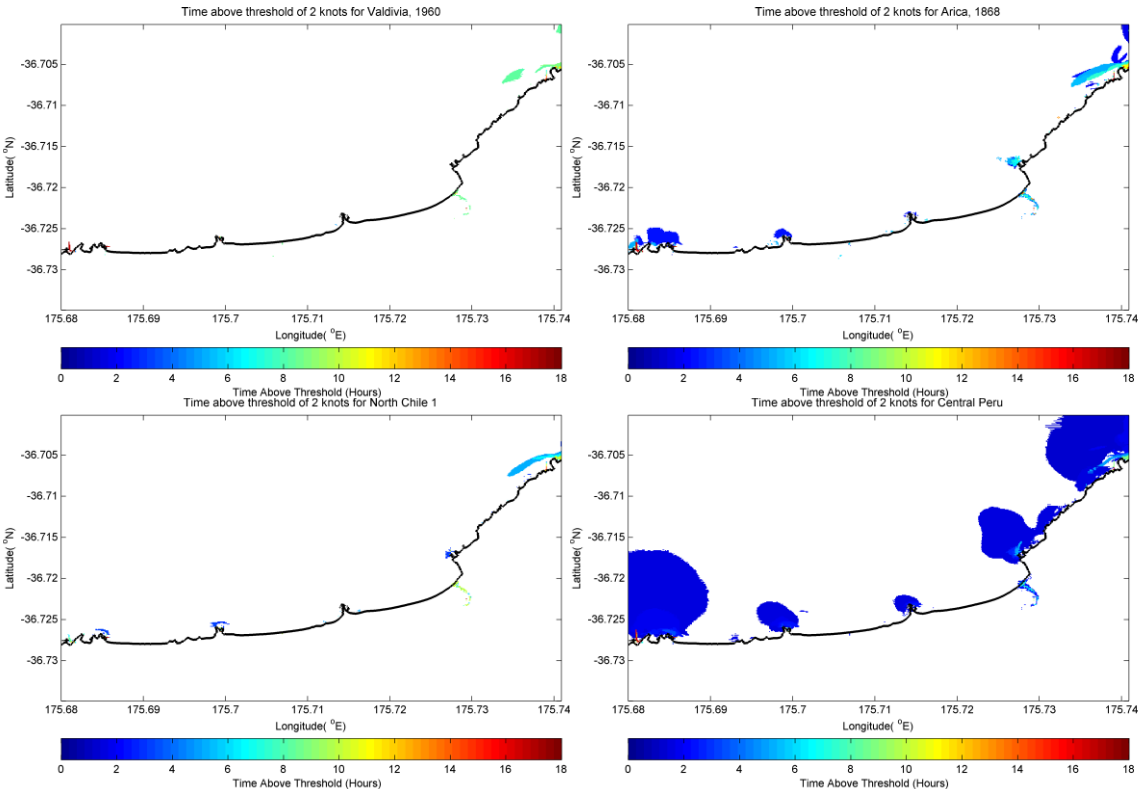

Figure 4.12 Time Current threshold maps for current speeds of 2 for the Chile 1960 (top left) Arica 1868 (top right), Chile North 1 (bottom left) and Central Peru (bottom right) at High tide in Kuaotunu.

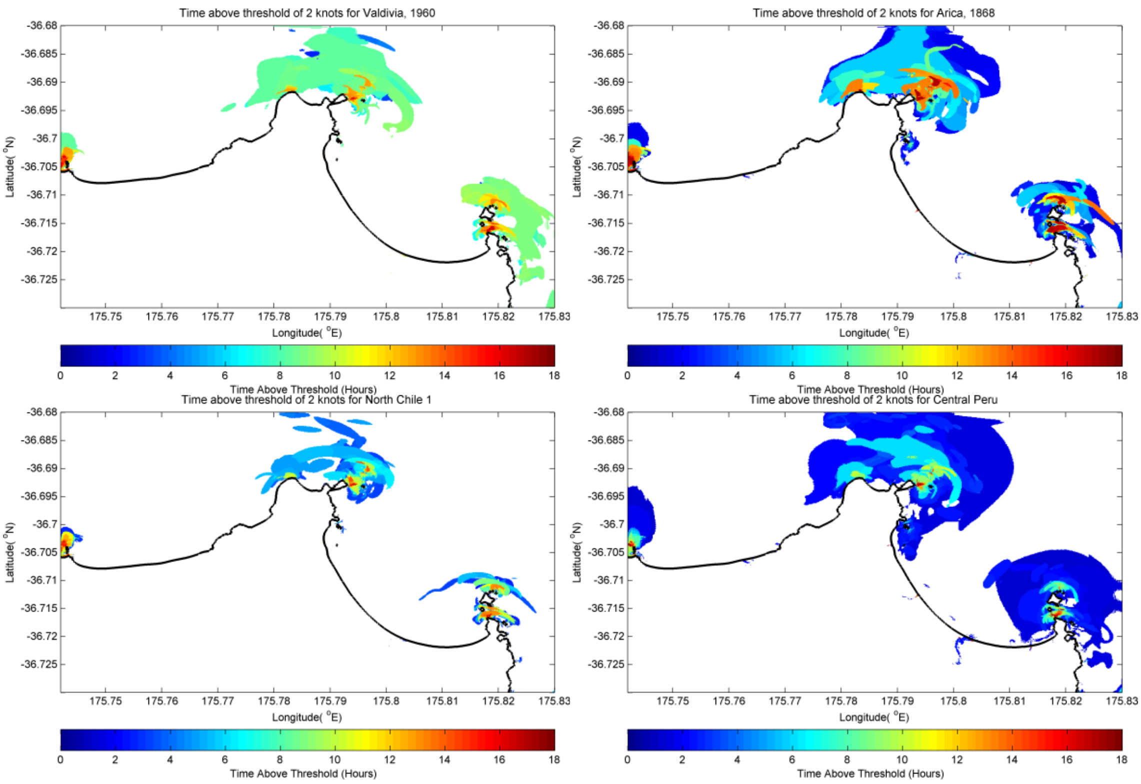

Figure 4.13 Time Current threshold maps for current speeds of 2 knots for the Chile 1960 (top left) Arica 1868 (top right), Chile North 1 (bottom left) and Central Peru (bottom right) at High tide in Opito Bay.

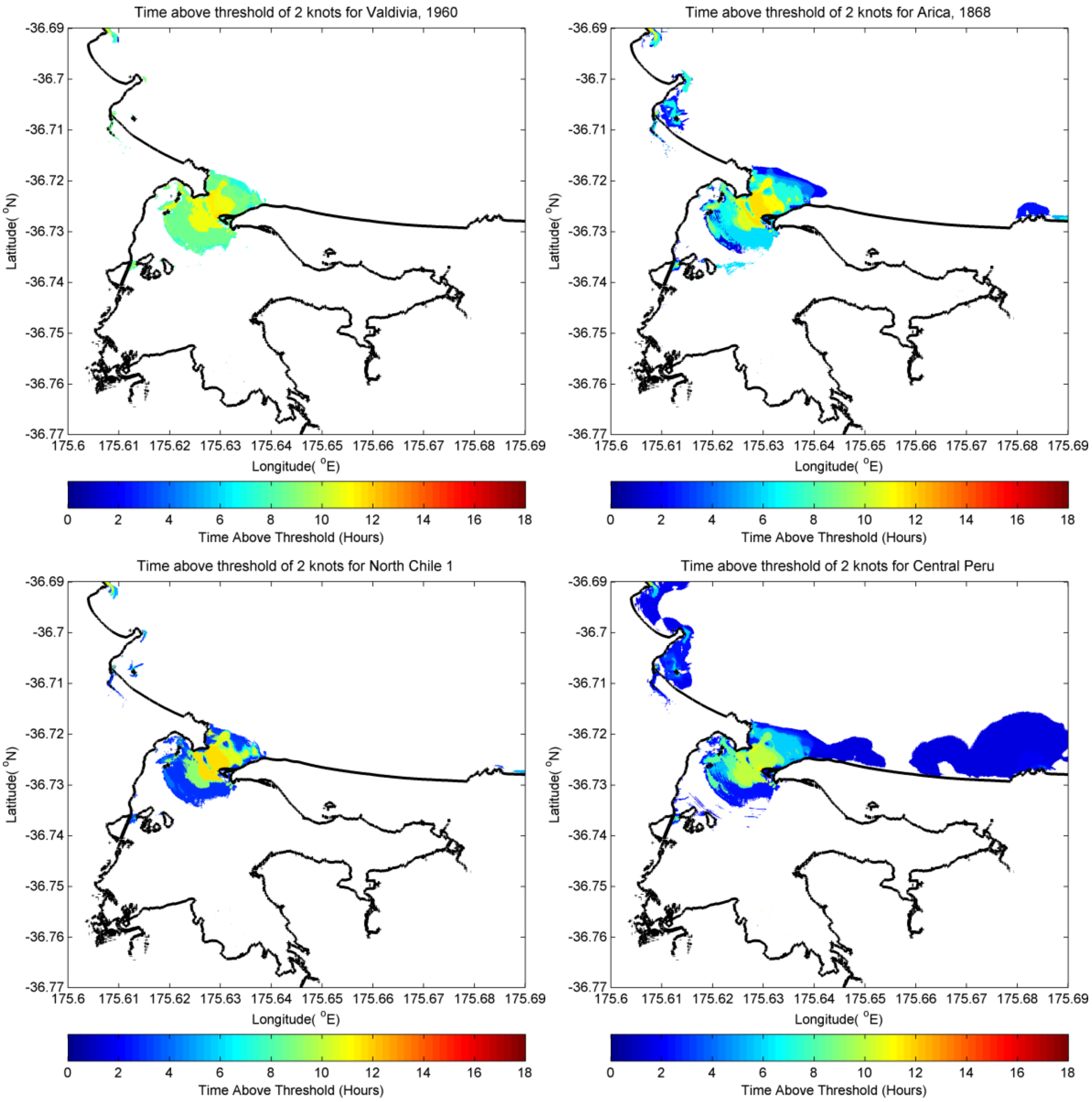

Figure 4.14 Time Current threshold maps for current speeds of 2 for the Chile 1960 (top left) Arica 1868 (top right), Chile North 1 (bottom left) and Central Peru (bottom right) at High tide in Whangapoua.

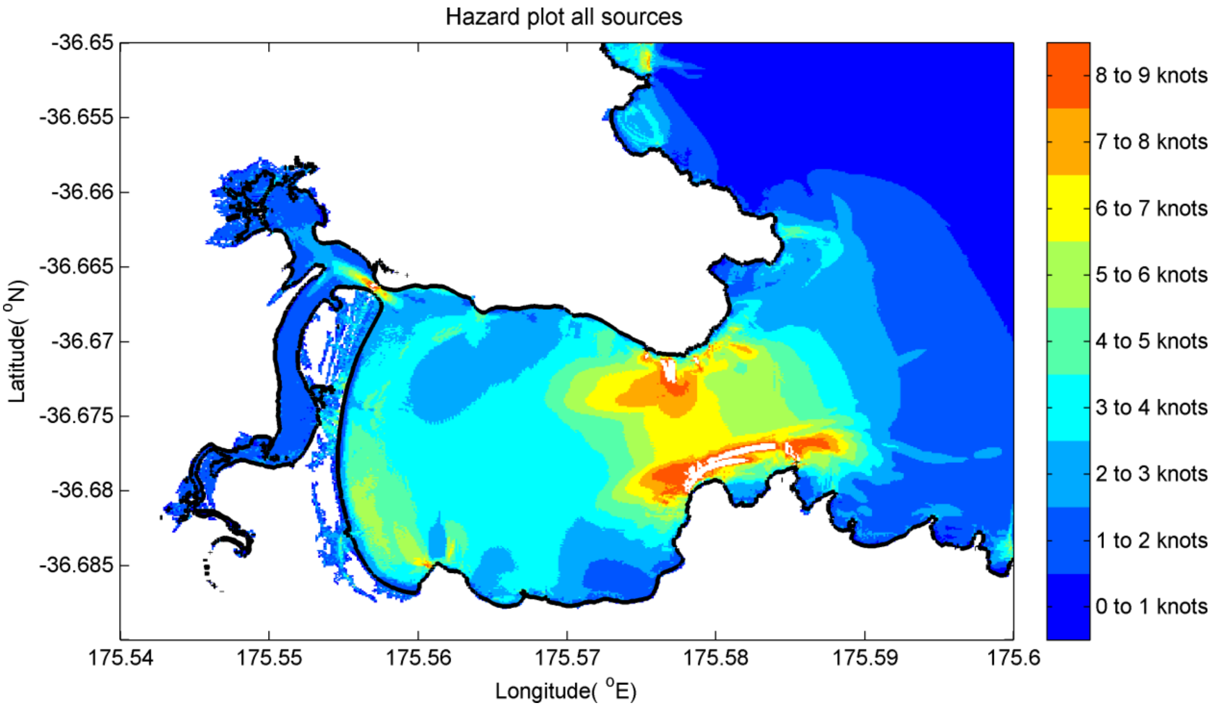
Hazard plot all sources
-36.65
-36.655
-36.66
-36.665
-36.67
-36.675
-36.68
-36.685
Latitude(°N)
175.54
175.55
175.56
175.57
175.58
175.59
175.6
Longitude(°E)
8 to 9 knots
7 to 8 knots
6 to 7 knots
5 to 6 knots
4 to 5 knots
3 to 4 knots
2 to 3 knots
1 to 2 knots
0 to 1 knots

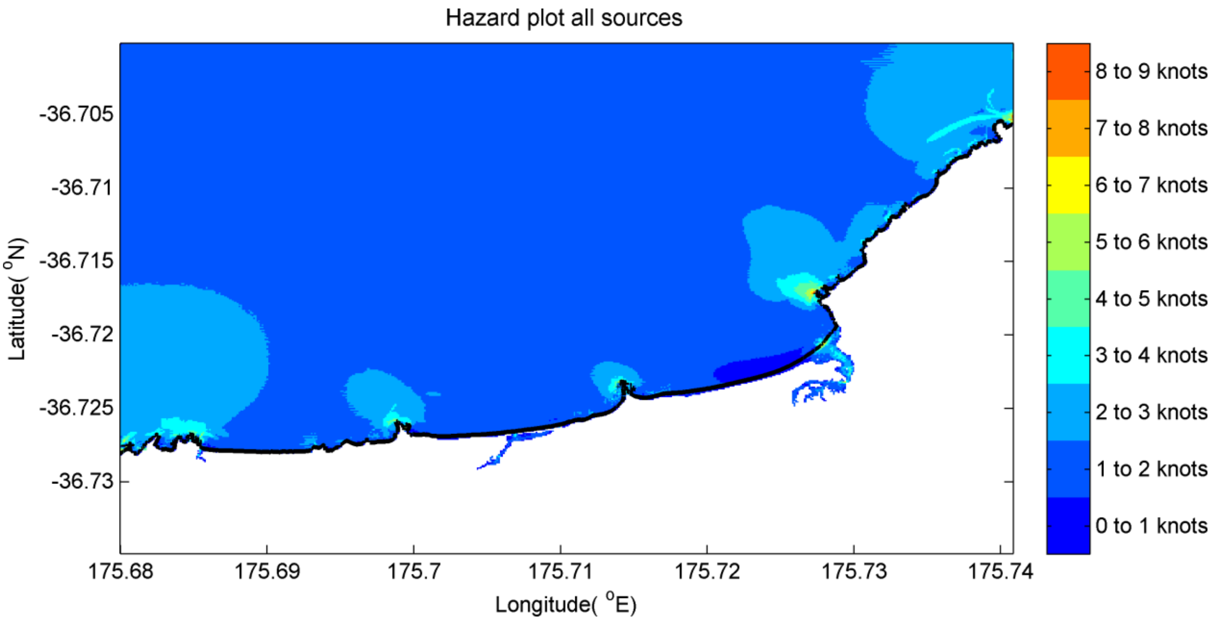
Hazard plot all sources
-36.705
-36.71
-36.715
-36.72
-36.725
-36.73
Latitude(°N)
175.68
175.69
175.7
175.71
175.72
175.73
175.74
Longitude(°E)
8 to 9 knots
7 to 8 knots
6 to 7 knots
5 to 6 knots
4 to 5 knots
3 to 4 knots
2 to 3 knots
1 to 2 knots
0 to 1 knots

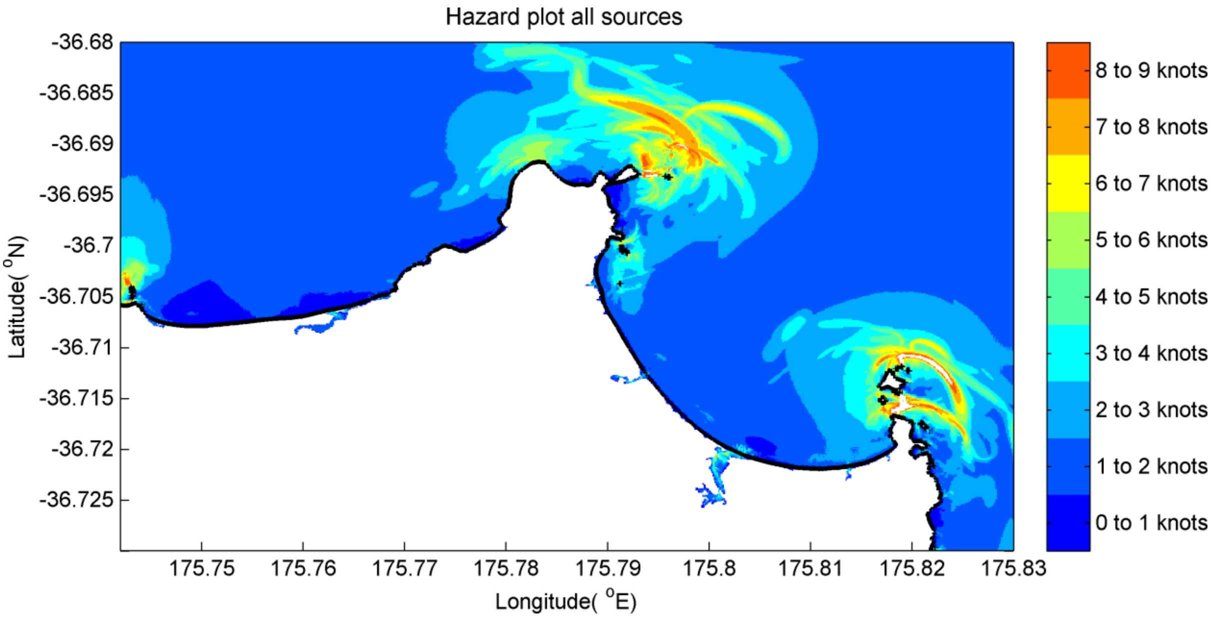

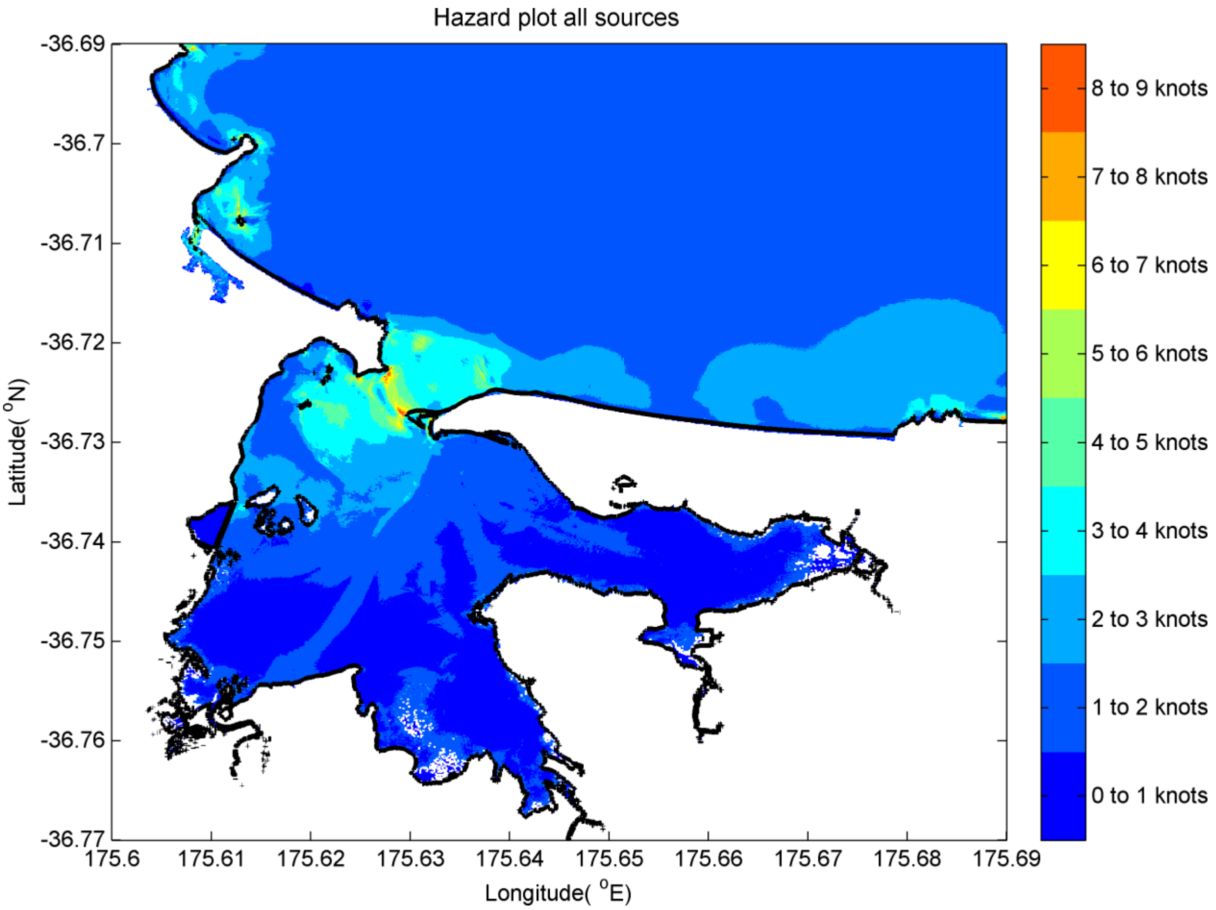

Figure 4.15 (above and previous page) Current hazard zones for the four C grid regions. Distant sources, high tide.

5 SUMMARY AND CONCLUSIONS

We have evaluated the tsunami hazard for Kennedy Bay, Whangapoua, Kuaotunu and Opito Bay for several near source and distant source tsunami scenarios. The assessment includes tsunami inundation, overland flow depths and tsunami induced current speeds.

For the regional sources we focus on the Tonga-Kermadec Trench and model a suite of 8 scenarios comprised of four different earthquakes at two different locations. Earthquake magnitudes range from M 8.8 to M 9.1 and consider both uniform and distributed slip scenarios. Of the cases modelled, only the three most extreme scenarios produce significant overland inundation at the study sites. All scenarios however produce potentially dangerous tsunami currents, particularly at the entrance to Kennedy Bay, Kennedy Bay estuary and Whangapoua estuary. The arrival time from these regional sources is quite short, from approximately 40 to 50 minutes for the initial withdrawal of the water level and between 60 to 90 minutes for the arrival of the first tsunami peak. Unlike the near source results for sites previously assessed on the eastern Coromandel Peninsula, the first wave was not the largest of the tsunami wave train. Furthermore, for these sites, the overall characteristics of the tsunami wave train were much more varied and complex with surges of significant height persisting for hours after tsunami arrival.

For the distant source scenarios, we consider several large magnitude (M 8.8 to 9.4) earthquake sources along the South American subduction zone. Three of these sources are based on Historical events (1868 Arica, 1960 Valdivia and 2010 Maule Chile events). The remaining four scenarios use an earthquake source model based on the 1960 Valdivia event that is positioned at different locations along the coast of South America. None of the scenarios tested produce large-scale inundation at Kennedy Bay, Whangapoua, Kuaotunu or Opito Bay. For all but one of the scenarios (Arica 1868), the peak tsunami wave height occurred more than 2 and as much as 8 hours after tsunami arrival. This is an important consideration for tsunami warnings for large, distant source events. In terms of tsunami induced current speeds, the distant source scenarios produce lower peak current speeds than the extreme regional source, however, the duration of the currents is much longer, with current speeds of more than 2 knots persisting for more up to 16 hours after tsunami arrival.

These model results will be used by the Thames-Coromandel District Council and the Waikato Regional Council as part of evacuation planning and emergency management activities as well as for education and outreach activities amongst the potentially affected populations.

6 REFERENCES

Borrero, J. C. (2013). *Numerical modelling of tsunami effects at two sites on the Coromandel Peninsula, New Zealand: Whitianga and Tairua-Pauanui* (No. 2013/24) (Vol. 4355, pp. 1–96).

Borrero, J. C. (2014). *Numerical modelling of tsunami effects at Whangamata, Whiritoa and Onemana, Coromandel Peninsula New Zealand*, Report prepared for the Waikato Regional Council, September 2014.

Borrero J.C. and Goring D.G (2015) South American Tsunamis in Lyttelton Harbor, New Zealand, *Pure and Applied Geophysics*, Volume 172, Issue 3, pp 757-772.

Borrero, J.C., Goring, D.G., Greer, S.D. and Power, W.L. (2014) Far-Field Tsunami Hazard in New Zealand Ports, *Pure and Applied Geophysics*, Volume 172, Issue 3, pp 731-756 .

De Lange, W. P., & Healy, T. R. (1986). New Zealand tsunamis 1840–1982. *New Zealand Journal of Geology and Geophysics*, *29*(1), 115–134. doi:10.1080/00288306.1986.10427527

Dorbath, L., A. Cisternas, and C. Dorbath (1990). Assessment of the size of large and great historical earthquakes in Peru, Bull. Seism. Soc. Am. 80, 551–576.

Fujii, Y., & Satake, K. (2012). Slip Distribution and Seismic Moment of the 2010 and 1960 Chilean Earthquakes Inferred from Tsunami Waveforms and Coastal Geodetic Data. *Pure and Applied Geophysics*, *170*(9-10), 1493–1509. doi:10.1007/s00024-012-0524-2

Gibson, F. (1868). On the Wave Phenomena observed in Lyttelton Harbor, August 15, 1868. *Transactions and Proceedings of the New Zealand Institute*, *1*, 195:196.

Power, W. L., & Gale, N. (2010). Tsunami Forecasting and Monitoring in New Zealand. *Pure and Applied Geophysics*, *168*(6-7), 1125–1136. doi:10.1007/s00024-010-0223-9

Power, W. L., Downes, G., & Stirling, M. (2007). Estimation of Tsunami Hazard in New Zealand due to South American Earthquakes. *Pure and Applied Geophysics*, *164*(2-3), 547–564. doi:10.1007/s00024-006-0166-3

Power, W. L., Wallace, L., Wang, X., & Reyners, M. (2011). Tsunami Hazard Posed to New Zealand by the Kermadec and Southern New Hebrides Subduction Margins: An Assessment Based on Plate Boundary Kinematics, Interseismic Coupling, and Historical Seismicity. *Pure and Applied Geophysics*, *169*(1-2), 1–36. doi:10.1007/s00024-011-0299-x

Prasetya, G. S., & Wang, X. (2011). *Tsunami frequency analysis for Eastern Coromandel and Waikato Region from Kermadec Trench and local sources within the Bay of Plenty* (No. 2011/135) (p. 65).

Titov, V. V., & González, Frank, I. (1997). *Implementation and testing of the Method of Splitting Tsunami (MOST) model* (No. ERL PMEL-112) (p. 14). Retrieved from http://www.pmel.noaa.gov/pubs/PDF/tito1927/tito1927.pdf

Titov, V. V., Moore, C. W., Greenslade, D. J. M., Pattiaratchi, C., Badal, R., Synolakis, C. E., & Kânoğlu, U. (2011). A New Tool for Inundation Modeling: Community Modeling Interface for Tsunamis (ComMIT). *Pure and Applied Geophysics*, *168*(11), 2121–2131. doi:10.1007/s00024-011-0292-4

Titov, V.V., and C.E. Synolakis (1995): Modeling of breaking and nonbreaking long wave evolution and runup using VTCS-2. J. Waterways, Ports, Coastal and Ocean Engineering, 121(6), 308–316.

Titov, V.V., and C.E. Synolakis (1997): Extreme inundation flows during the Hokkaido-Nansei-Oki tsunami. Geophys. Res. Lett, 24(11), 1315–1318.